COST Action 710

Harmonization in the Preprocessing of Meteorological Data for Atmospheric Dispersion Models

Report of Working Group 1

SURFACE ENERGY BALANCE

Ulrike Pechinger (chairman)

Ernst Dittmann

Gerhard Erbes

Per-Erik Johansson

Ari Karppinen

Luc Musson-Genon

Gunnar Omstedt

Philippe Tercier

December 1997

Ulrike Pechinger:	Central Institute for Meteorology and Geodynamics, Vienna, Austria
Gerhard Erbes:	Central Institute for Meteorology and Geodynamics, Vienna, Austria
Per-Erik Johansson:	Division of Environment and Protection, National Defence Research Establishment, Umea, Sweden
Ari Karppinen:	Finnish Meteorology Institute, Helsinki, Finland
Luc Musson-Genon:	EDF/DER/ENV, Chatou Cedex, France
Gunnar Omstedt:	Swedish Meteorology Institute, Norrköping, Sweden
Philippe Tercier:	Swiss Meteorology Institute, Payerne, Switzerland

COST 710 WORKING GROUP 1 - SURFACE ENERGY BALANCE

List of Figures

Fig. 4.3.2.2: Sensible heat flux, with the following comparisons: a) OML-Marsta, b) FMI-Marsta, c) OML-Tisby, d) FMI-Tisby, e) OML-FMI, and f) Marsta-Tisby. The correlation coefficients are given by R.

Fig. 4.3.2.3: Net radiation, with the following comparisons: a) OML-Marsta, b) FMI-Marsta, c) OML-Tisby, d) FMI-Tisby, e) OML-FMI, and f) Marsta-Tisby. The correlation coefficients are given by R.

Fig. 4.3.2.4: Inverse Monin-Obukhov length frequencies for the following: a) Marsta, b) Tisby, c) OML, and d) FMI.

Fig. 4.4.1: Diurnal variations of the measured (dashed lines) and the calculated (solid lines) ground heat flux at the surface. Comparison for three days and 5 methods.

Fig. 4.4.2: **Left**: depth in the soil at wich the diurnal amplitude of the temperature is equal to one degree C for a given amplitude at the surface and for 3 values of the soil thermal diffusivity. **Right:** annual variation of temperature in the soil, ANETZ-station Payerne (average over 6 years)

Fig. 4.4.3: **Left:** ground heat flux at the surface determined from measured net radiation with the commonly proposed proportionality factors of 0.1 for the day and 0.5 for the night versus measured ground heat flux at the surface. **Right:** linear best fit between measured net radiation and measured ground heat flux at the surface. The day-night limit is given by the value of the total incoming radiation > 5 W/m^2. Measurements taken at Payerne from August 1995 to July 1996.

Fig. 4.4.4: **Left:** ground heat flux at the surface determined with the force-restore method using a sinusoidal function for T_m versus measured ground heat flux at the surface. **Right:** same as left, but using the measured soil temperature at 10 cm for T_m. Measurements taken at Payerne from August 1995 to July 1996.

Fig. A 1: Global mean surface energy budget averaged over the 4 seasons. CI is an annual mean climatology prepared by Ramanathan et.al. (1989), CI2 are climotological values from Morel (1994). E is ECMWF, J JMA, N NMC(USA), U UKMO, SH sensible heat, LH latent heat, NSW net shortwave radiation, NLW net longwave radiation, NHF net heat flux. Upward fluxes indicated by a hyphen after abbreviation.

List of Tables

List of Abbreviations and Symbols

1. Abbreviations

ABL	Atmospheric Boundary Layer
CBL	Convective Boundary Layer
ETP	Evening Transition Period
EZ	Entrainment Zone
ML	Mixing Layer
MH	Mixing Height
MOST	Monin-Obukhov Similarity Theory
MTP	Morning Transition Period
LES	Large-Eddy Simulation
LLJ	Low-Level Jet
SBL	Stable Boundary Layer
SL	Surface Layer
SR	SunRise
SS	SunSet
TKE	Turbulent Kinetic Energy

2. Symbols

A	(surface) albedo
A_μ, B_μ, C_μ	universal functions in resistance and heat transfer laws
Bo	Bowen ratio
C_D, C_G, C_H	drag ~, geostrophic drag ~ and bulk heat transfer coefficients
C_T^2, C_V^2, C_N^2	structure parameters for temperature ~, wind velocity ~ and refractive index fluctuations
c_p	specific heat at constant pressure
D	direct beam incoming shortwave radiation
Ds	diffuse incoming shortwave radiation
d	displacement height
E	turbulent kinetic energy
e, e_S	water vapour pressure, saturation water vapour pressure
f	Coriolis parameter
g	acceleration of gravity
H	sensible heat flux
h	mixing height
I_0	solar constant
K_H, K_M	turbulent exchange coefficients (eddy diffusivities) for heat and momentum
$K\uparrow$	outgoing shortwave radiation
K*	net shortwave radiation
k	(spectral) wave number ($k = 2\pi / \lambda$)
L	any length scale

L_*	Monin-Obukhov length ($L_* = - u_*^3 / (\langle w'\Theta' \rangle_0 \kappa \beta)$
$L\downarrow$	incoming longwave radiation
$L\uparrow$	outgoing longwave radiation
L^*	net longwave radiation
$\mathcal{L}E$	latent heat flux
l	mixing length
ℓ_v	latent heat of evaporation
m	mass
N_{BV}	Brunt-Väisälä frequency ($N_{BV} = (\beta\gamma_\Theta)^{1/2}$)
N_C	fractional cloud cover
Pr	Prandtl number ($Pr = K_M/K_H$)
p	air pressure
Q_G	ground heat flux
q	specific humidity
R_g	global radiation
R_n	net radiation
RH	relative humidity
Ri	Richardson number (general)
Ri_b, Ri_g, Ri_f	bulk / gradient / flux Richardson number
R_{net}	net radiation
r	mixing ratio
S	sodar backscattered sound signal intensity
T	temperature
T_d	dewpoint temperature
T_e	Eulerian time scale of atmospheric turbulence
T_l	Lagrangian time scale of atmospheric turbulence
t	time
u, v	x, y-components of the horizontal wind vector
u_g, v_g	x, y-components of the geostrophic wind vector
u_*	friction velocity
V	(horizontal) wind speed
V_g	geostrophic wind speed
w	vertical wind component
w_s	large-scale vertical velocity
w_*	convective scaling velocity ($w_* = (\beta\, h\, \langle w'\Theta' \rangle_0)^{1/3}$)
z	height coordinate
z_i	base level height of an elevated inversion
z_0	roughness length
α	Priestley-Taylor parameter
α	wind direction
α_H, α_M, α_W	exponents in the similarity relationships for the vertical profiles of $\langle w'\Theta' \rangle_0$, τ, and σ_w^2
β	buoyancy parameter ($\beta = g / T$)

$\beta_{H,M}$	parameter in the MOST universal functions for the profiles of temperature and wind
γ, γ_Θ	vertical gradient of temperature / potential temperature
ε	TKE dissipation rate
Θ, Θ_v	potential and virtual potential temperature
Θ_*	temperature scale ($\Theta_* = - \langle w'\Theta' \rangle_0 / u_*$ in the SL and $\Theta_* = - \langle w'\Theta' \rangle_0 / w_*$ in the CBL)
θ_z	zenith distance angle
κ	von-Kármán constant ($\kappa = 0.4$)
λ	wavelength
ς, ς_h	stability parameter ($\varsigma = z/L$ or $\varsigma_h = h/L$)
ρ	air density
σ_α	standard deviation of wind direction fluctuations
σ_{v_2}	standard deviation of lateral wind speed fluctuations
σ_w^2	vertical velocity variance
τ	shear stress
ϕ	geographical latitude
Φ_H, Φ_M	MOST stability functions
ω	angular rotation of the earth
$\langle w'\Theta' \rangle$	kinematic (potential) temperature flux

In addition, the following notations will be applied:

Index "0" refers to values determined at the earth surface (or within the surface layer)
Index "h" refers to values at height z = h.
Values averaged over the whole mixed layer are characterized by an overbar ("¯").
Angle brackets ⟨ ⟩ indicate an ensemble average.

Additional list of symbols

R_n	$W\ m^{-2}$	net radiation (at ground level, all wave lengths)
G	$W\ m^{-2}$	incoming short-wave or global radiation
$K\uparrow$	$W\ m^{-2}$	outgoing short-wave radiation
$L\downarrow$	$W\ m^{-2}$	incoming long-wave radiation
$L\uparrow$	$W\ m^{-2}$	outgoing long-wave radiation
H	$W\ m^{-2}$	sensible heat flux
Q_E	$W\ m^{-2}$	latent heat flux
Q_G	$W\ m^{-2}$	ground heat flux
Λ		albedo
K*	$W\ m^{-2}$	net short-wave radiation
L*	$W\ m^{-2}$	net long-wave radiation
ε		emissitivy
σ	$W\ m^{-2}\ K^{-4}$	Stefan-Boltzmann constant
Bo		Bowen's
λ_s	$W\ m^{-1}\ K^{-1}$	thermal conductivity of the soil
T_s	K	soil temperature
ρ_s	$kg\ m^{-3}$	soil density
c_s	$J\ kg^{-1}\ K^{-1}$	specific heat capacity of the soil

Additional list of symbols

$\langle w'u' \rangle_o$	kinematic wind flux
$\langle w'q' \rangle_o$	kinematic specific humidity flux
Ψ_m, Ψ_h	integrals of most stability functions
P_{tN}	neutral turbulent Prandtl number
$\Delta u, \Delta\theta$	wind, potential temperature differences between two levels in the SL
C_D, C_H	wind and temperature drag coefficient
Ri_b	bulk Richardson number
z_{ot}	thermal roughness height

α_s	(modified) Priestley-Taylor parameter
β_s	coefficient in modified Priestley-Taylor formula
N_{tot}	total cloud cover in octas
N_l	amount of low clouds in octas
N_m	amount of medium-high clouds in octas
N_h	amount of high clouds in octas
r_a	aerodynamic resistance
r_s	surface resistance
Δ	the gradient of the saturated vapour pressure with respect to temperature
γ_p	the psychrometric constant
q_s	the satured specific humidity

1. INTRODUCTION

Models for calculating short-range dispersion from point sources for regulatory purposes require information on the state of the atmospheric boundary layer from standard meteorological data. While traditional Gaussian plume models still use simple stability classification schemes based on routinely available measurements to describe the state of the atmosphere, recent dispersion models require more sophisticated information on the state of the boundary layer.

Many atmospheric dispersion models use similarity theories to calculate the necessary dispersion parameters. Measurements of the surface fluxes of momentum and heat are needed to use the similarity approach. Such measurements, however, are not routinely available. Thus meteorological preprocessors have been developed to estimate the surface fluxes from routinely available observations like cloud cover, wind speed, temperature, etc.

The COST 710 - action "Harmonization in the Preprocessing of Meteorological Data for Atmospheric Dispersion Models" is a European wide project to test, compare and harmonize some of the sub-modules entering these diffusion models.

Working group 1 of COST 710 has addressed the methods for calculating the surface energy balance and for parameterizing the atmospheric heat and momentum fluxes and the ground heat flux. Meteorological data needed for input and evaluation are discussed. Two commonly used preprocessors in European dispersion models are the schemes suggested by Berkowicz and Prahm, 1982 (BP) and Holtslag and van Ulden 1982,1983 (HU). In various studies in the present report these schemes (in various implementations) are intercompared and compared against data. The determination of roughness length, net radiation and soil moisture is not addressed.

The report is structured as follows:

Chapter 2 contains a description of different models for calculating the surface energy balance (with a description of the profile method for the determination of fluxes in the surface layer) and an overview on measuring and modelling the ground heat flux. As examples of the resistance method the BP and HU heat flux schemes are described. The BP scheme is in use at the Swedish Meteorological Institute. At the Finnish Meteorological Institute a modification of the HU scheme for application at high latitude regions is used.

Chapter 3 summarizes the necessary meteorological data needed as input for the profile method, for the resistance method and for numerical weather prediction models. Also the kind of data that is needed for the evaluation of the meteorological preprocessors, is addressed. The use of satellite data for model input and evaluation is discussed.

Chapter 4 presents intercomparison studies carried out within the WG 1 of COST 710:

- In one study, the Finnish and the Swedish schemes (based on th HU and BP schemes, respectively) were intercompared. This study aimed to investigate the properties of the two schemes relative to each other and did not involve direct comparisons with observations. One year of data from Southern Finland was used to derive frequency distributions etc.
- The Finnish and the Swedish schemes were intercompared with 3 months of meteorological data collected under stable, low wind speed winter conditions and snow covered surface at Umeå airport in Sweden. The BP and the HU scheme have been developed for mid-latitudes with grass covered surfaces. One of the questions was, how well they would perform for such typical Northern European winter conditions.
- To extend these comparisons both schemes were also intercompared with 4 months of data for high-latitude spring and summer conditions obtained from the NOPEX campaign.
- A comparison of the profile method and the resistance method was also carried out with data from the surroundings of Paris during a pollution episode.
- Daily variations of the soil heat fluxes calculated with 5 different methods are compared with Swiss data for three selected days.
- A statistical analysis of calculated and measured soil heat fluxes is carried out for one year of data from Switzerland.

Limitations concerning the use of the different methods, the determination of some of the boundary layer parameters and the siting of instruments is addressed in chapter 5.

Chapter 6 is a summary, while chapter 7 provides also recommendations regarding the use of the methods, improvements of measurement and data sets. Various additional material is contained in chapters 8 to 10 (references, a list of available data sets and a list of preprocessing methods with available programs).

2. OVERVIEW OF METHODS AND MODELS

The basic formula for the surface energy balance is

$$R_n = H + Q_E + Q_G \qquad (2.1)$$

where R_n is the net radiation, H the sensible heat flux, Q_E the latent heat flux, and Q_G the ground heat flux. Methods and models, described in this chapter, deal with the evaluation of the components of equation (2.1) and their partitioning. The components of Equation (2.1) are important in order to use the similarity approach for calculating dispersion parameters.

The *profile method* is used to determine the turbulent sensible heat flux using the universal functions of wind speed and temperature for the surface layer of the atmospheric boundary layer according to the Monin Obukhov similarity theory. The latent heat flux may be calculated by analogy, depending on the availability of humidity data at different heights within the surface layer.

The *resistance method* estimates the net radiation by using regression relations with cloud cover, solar elevation and sometimes additionally with air temperature, wind speed and global radiation. Then, relations similar to Ohm's resistance law are used to calculate the sensible and latent heat fluxes. The resistance to the fluxes is split into an aerodynamic and a surface part.

The ground heat flux often is calculated as a proportional part of the net radiation. But there are more refined methods and models for this component of the surface energy balance equation, as shown in chapter 2.3.

2.1 THE PROFILE METHOD

2.1.1 Similarity profiles

The profile method is commonly used to determine fluxes in the Surface Layer (SL) of the atmospheric boundary layer.

This method uses the SL laws deduced from the Monin Obukhov similarity theory in order to determine the fluxes of sensible heat and momentum on the basis of differences of wind and temperature between two different levels.

In this theory, gradients of the mean parameters can be expressed in terms of universal functions depending on $\frac{z}{L_*}$, where L_* is the Monin-Obukhov length and z the altitude.

For wind speed and temperature, one obtains the following well-known relationships:

$$\begin{cases} \dfrac{\partial u(z)}{\partial z} = \dfrac{u_*}{\kappa z}\Phi_m\left(\dfrac{z}{L_*}\right) & (2.1.1) \\ \dfrac{\partial \theta(z)}{\partial z} = \dfrac{\theta_*}{\kappa z}\Phi_h\left(\dfrac{z}{L_*}\right) & (2.1.2) \end{cases}$$

with:

$$\begin{cases} u_* = \sqrt{\langle w'u' \rangle_o} & (2.1.3) \\ \theta_* = -\dfrac{\langle w'\theta' \rangle_o}{u_*} & (2.1.4) \\ L_* = \dfrac{\overline{\theta}\, u_*^2}{\kappa g\, \theta_*} & (2.1.5) \end{cases}$$

where θ is the potential temperature, $\overline{\ }$ average in the SL and θ_* a temperature scale.

u_* is the friction velocity

L_* is the Monin Obukhov length. More precisely, the Monin Obukhov length depends on humidity and θ_* has to be replaced by $\theta_* + 0.608\,\overline{\theta} q_*$ where $q_* = -\dfrac{\langle w'q' \rangle_o}{u_*}$ but, practically, this correction is often neglected even if this approximation could be less precise when evaporation processes are predominant.

In order to simplify the presentation, humidity profiles and fluxes are not described here but it is easy to express them by assuming that humidity obeys the same laws than temperature.

The functions Φ_m and Φ_h are universal functions of $\frac{z}{L_*}$. There have been many experiments to determine them.

2.1.2 The universal functions

The Monin-Obukhov similarity theory has been widely used in meteorology to study the SL. Numerous works and measurement campaigns have been carried out in order to determine the universal functions for the wind (Φ_m), for the temperature (Φ_h) as well as for the humidity (Φ_q), which can be written in the following form:

unstable case

$$\Phi_m = (1. - \gamma_1 \zeta)^{\frac{-1}{4}} \qquad (2.1.6)$$

$$\Phi_h = P_{tN} (1. - \gamma_2 \zeta)^{\frac{-1}{2}} \qquad (2.1.7)$$

stable case

$$\Phi_m = 1. + \beta_{1M} \zeta, \qquad (2.1.8)$$

$$\Phi_h = P_{tN} + \beta_{1H} \zeta \qquad (2.1.9)$$

Despite that, there is still disagreement on the coefficients of these functions. Wieringa (1980) and Högström (1987) suggested that these differences were probably due to experimental errors caused by disturbance of the flow by the instrumentation. They propose new formulations with a reevaluation of the Karman constant coherent with the correction of the other constants.

Values for the different constants entered into the calculation of (Φ_m) and (Φ_h), based on atmospheric observations and the Dyer (1974) review, are presented in Table I taken from Garratt (1994).

Table 1: Values of surface-layer constants, where κ is the von Karman constant, P_{tN} is the neutral turbulent Prandtl number and β and γ are experimental constants appearing in the expressions for the Monin-Obukhov stability functions (Φ_m) and (Φ_h)

	κ	P_{tN}	γ_1	γ_2	β_{1M}	β_{1H}
Observations						
Webb (1970)	-	-	-	-	5.2	5.2
Dyer and Hicks (1970)	0.41	1	16	-	-	-
Businger et al. (1971)	0.35	0.74	15	9	4.7	4.7
Garrat (1977)	0.41	-	-	-	-	-
Wieringa (1980)	0.41	1	22	13	6.9	9.2
Dyer and Bradley (1982)	0.4	1	28	14	-	-
Webb (1982)	-	1	20.3	12.2	-	-
Hogstrom (1985)	0.4	1	-	-	4	-
Hogstrom (1988)	0.4	0.95	19	11.6	6.0	7.8
Zhang et al. (1988)	0.4	-	-	-	-	-
Review						
Dyer (1974)	0.41	1	16	16	5	5

2.1.3 Determination of the fluxes

The sensible heat flux is given by:

$$H = -\rho c_p u_* \theta_* \tag{2.1.10}$$

The unknown u_*, H and L_* can be directly evaluated from these relations but a direct determination of the gradients would require too many measurements with a very good accuracy and it is in fact not practicable. One prefers to integrate these expressions between the roughness height z_0, where the wind is equal to zero, to a height z :

$$u(z)=\frac{u_*}{\kappa}\left[\ln\frac{z}{z_0}-\Psi_m\left(\frac{z}{L_*}\right)+\Psi_m\left(\frac{z_0}{L_*}\right)\right] \tag{2.1.11}$$

$$\theta(z)-\theta(z_{0t})=P_{tN}\frac{\theta_*}{\kappa}\left[\ln\frac{z}{z_{0t}}-\Psi_h\left(\frac{z}{L_*}\right)+\Psi_h\left(\frac{z_{0t}}{L_*}\right)\right] \tag{2.1.12}$$

where P_{tN} (0.74 according to the relations of Businger et al. (1971)) is the neutral turbulent Prandtl number.

Using the universal functions of Businger et al. (1971), Paulsen (1970) and Barker and Baxter (1975) obtained the following functions:

$$\Psi_m(\zeta)=\ln\left[\left(\frac{1+x}{2}\right)^2\left(\frac{1+x^2}{2}\right)\right]-2\arctan x+\frac{\pi}{2} \qquad \text{for } \zeta<0 \tag{2.1.13a}$$

$$\text{with } x=(1-15\zeta)^{\frac{1}{4}}$$

$$\Psi_m(\zeta)=-4.7\zeta \qquad \text{for } \zeta>0 \tag{2.1.13b}$$

$$\Psi_h=2\ln\left[\frac{1+y}{2}\right] \qquad \text{for } \zeta<0 \tag{2.1.14a}$$

$$\text{with } y=(1-9\zeta)^{\frac{1}{2}}$$

$$\Psi_h(\zeta)=-\frac{4.7}{P_{tN}}\zeta \qquad \text{for } \zeta>0 \tag{2.1.14b}$$

In fact if the values of the temperature and of the wind velocity at two different levels are available, it is possible to perform the integration between any two levels. These levels can be independent.

With zu_1 and zu_2 two wind speed levels, and zt_1 and zt_2 two temperature levels, the complete system to be solved is:

$$\begin{cases} \Delta u = \dfrac{u_*}{\kappa}\left[\ln\left(\dfrac{zu_2}{zu_1}\right) - \Psi_m\left(\dfrac{zu_2}{L_*}\right) + \Psi_m\left(\dfrac{zu_1}{L_*}\right)\right] & (2.1.15a) \\ \Delta\theta = \dfrac{P_{iN}\theta_*}{\kappa}\left[\ln\left(\dfrac{zt_2}{zt_1}\right) - \Psi_h\left(\dfrac{zt_2}{L_*}\right) + \Psi_h\left(\dfrac{zt_1}{L_*}\right)\right] & (2.1.15b) \\ L_* = \dfrac{\bar{\theta}\, u_*^2}{g\,\kappa\theta_*} & (2.1.15c) \\ H = -\rho c_p u_*\theta_* & (2.1.15d) \end{cases}$$

with $\Delta u = u(zu_2) - u(zu_1)$ and $\Delta\theta = \theta(zt_1) - \theta(zt_2)$

Eliminating u_* and θ_* from the equations (2.1.15a) and (2.1.15b) and by substituting them into (2.1.15c), one obtains:

$$L_* = \left[\frac{\bar{\theta}\,\Delta u^2}{g\,\Delta\theta}\right] P_{iN} \times \left\{\frac{\ln\left(\dfrac{zt_2}{zt_1}\right) - \Psi_h\left(\dfrac{zt_2}{L_*}\right) + \Psi_h\left(\dfrac{zt_1}{L_*}\right)}{\left[\ln\left(\dfrac{zu_2}{zu_1}\right) - \Psi_m\left(\dfrac{zu_2}{L_*}\right) + \Psi_m\left(\dfrac{zu_1}{L_*}\right)\right]^2}\right\} \qquad (2.1.16)$$

At this point, two solutions are possible. The less restrictive one is to solve this system of equations with an iterative procedure.

2.1.3.1 The iterative solution

The algorithm for this iterative solution can be expressed following Berkowicz and Prahm (1982 a):

Step A: u_* and θ_* are calculated from the equations (2.1.15 a) and (2.1.15 b) and by taking $\frac{z}{L_*} = 0$.

Step B: L_* is calculated from (2.1.15 c) using the previous values of u_* and θ_*.

Step C: L_* is reintroduced in (2.1.15 a) and (2.1.15 b) and u_* and θ_* are computed.

Step D: steps B and C are repeated until the variation in L_* is smaller than the required accuracy.

This procedure converges in the unstable case but not in the case of very stable conditions when the Richardson number is greater than a critical value depending on the function used (e.g. 0.21 for the given ϕ function). In that case, a common practice is to maintain turbulence by using values corresponding to the critical Richardson number.

2.1.3.2 The analytical solution (Louis , 1979)

This method is essentially used in numerical simulation where iterative procedures are computationally expensive.

By taking $zu2 = zt2 = z2$, $zu1 = zt1 = z1$, the Monin Obukhov length can be determined as a function of the bulk Richardson number $Ri_b = \frac{g(z_2 - z_1)\Delta\theta}{\bar{\theta}\,\Delta u^2}$

In that case, equation (2.1.16) can be reduced to an explicit relation between L. and Ri_b:

$$\frac{L_*}{z} = F\left(\frac{z}{z_o}, Ri_b\right) \qquad (2.1.17)$$

which can be written with a change of origin for z:

$$C_D = \frac{u_*^2}{u^2} = a^2 F_d\left(\frac{z+z_o}{z_o}, Ri_b\right)$$

$$C_H = P_{rN}\frac{\theta_* u_*}{u\Delta\theta} = a^2 F_h\left(\frac{z+z_o}{z_o}, Ri_b\right) \qquad (2.1.18)$$

where $a = \frac{k}{\ln\left(\frac{z+z_o}{z_o}\right)}$

a^2 is the neutral drag coefficient for momentum.

The F_d and F_h functions depend on stability and checked in order to be close to the iterative solution.

unstable case:
In order to be coherent at the limit of free convection, C_D and C_H have to behave asymptotically as $(Ri_b)^{\frac{1}{2}}$. Moreover, continuity is assumed through neutrality with a slope more pronounced for wind than for temperature. That gives the following expressions (Louis et al, 1982):

$$C_D = a^2\left(1 - \frac{2bRi_b}{1 + 3a^2bc\sqrt{\frac{z+z_o}{z_o}|Ri_b|}}\right) \qquad (2.1.19)$$

unstable case

$$C_H = a^2\left(1 - \frac{3bRi_b}{1 + 3a^2bc\sqrt{\frac{z+z_o}{z_o}|Ri_b|}}\right) \qquad (2.1.20)$$

with b = c = 5

In stable case the turbulence can be forced for Richardson number values greater than the value of the critical Richardson number. That gives the following expressions:

$$C_D = a^2 \left(\frac{1}{1 + \frac{2 b R i_b}{\sqrt{1 + d R i_b}}} \right) \qquad (2.1.21)$$

stable case

$$C_H = a^2 \left(\frac{1}{1 + 2 b R i_b \sqrt{1 + d R i_b}} \right) \qquad (2.1.22)$$

with b = d = 5.

With this system it is possible to obtain directly the fluxes and the Monin Obukhov length but one needs to know wind and temperature at the same levels.

2.1.3.3 Beljaars and Holtslag (1991) formulation

The disadvantage of the previous functions is that they have not been checked under conditions of very high stability. In that case, turbulence decays for R_{ib} greater than 0.21 and unrealistic results are obtained in numerical weather prediction because the surface tends to become thermally discoupled from the atmosphere producing too strong a cooling of the earth's surface.
To avoid some of these problems, Beljaars and Holtslag (1991) proposed for the integral of Φ_m and Φ_h functions Ψ_m and Ψ_h a new formulation for the stable case, while keeping Dyer's (1974) relationships in the case of unstable stratification:

Unstable case:

$$\Psi_m = 2 \ln\left(\frac{1+x}{2}\right) + \ln\left(\frac{1+x^2}{2}\right) - 2 \arctan(x) + \frac{\pi}{2} \qquad (2.1.23)$$

$$\Psi_{h,q} = 2 \ln\left(\frac{1+x^2}{2}\right) \qquad (2.1.24)$$

where $x = (1-16\zeta)^{\frac{1}{4}}$

Stable case:

$$\Psi_m = -\left[a\zeta + b\left(\zeta - \frac{c}{d}\right)\exp(-d\zeta) + \frac{b\,c}{d}\right] \tag{2.1.25}$$

$$\Psi_{h,q} = -\left[\left(1+\frac{2\,a}{3}\zeta\right)^{\frac{3}{2}} + b\left(\zeta - \frac{c}{d}\right)\exp(-d\zeta) + \frac{b\,c}{d} - 1\right] \tag{2.1.26}$$

where a=1 b=0.667 c=5 d=0.35

The results obtained with these functions are close to that obtained with Hogstrom's (1988) proposition in their range of validity. The differences with Louis et al (1982) formulation are more pronounced especially in stable conditions where Louis et al (1982) formulation seems to overestimate momentum transfer coefficient (Beljaars and Holtslag, 1991).
In their paper, they show that an effective roughness height for momentum is needed to parameterize the momentum flux at horizontal scale of a few kilometers and that it is important to take into account thermal roughness in the sensible heat flux estimation.

2.2 THE RESISTANCE METHOD

The resistance method is a combination method where use is made of the surface energy balance equation, relationships between fluxes and gradients of mean quantities and knowledge about the surface condition. Galinski and Thomson (1995) have made an comparison between three different methods against data from England. These methods have been designed to be applicable to mid-latitude, grass covered surfaces. For this review only two of them will be discussed i.e. the Berkowicz and Prahm heat flux method (1982) and the Holtslag and van Ulden heat flux method (1982,1983).

The starting point is the equation of the surface energy balance

$$R_n = Q_E + H + Q_G \qquad (2.2.1)$$

where R_n is the net radiation, Q_E is the latent heat flux, H the sensible heat flux and Q_G the soil heat flux.

The net radiation, R_n, is the balance between downward and upward short-wave and long-wave radiations. In the Berkowicz and Prahm method the net radiation is estimated following Nielsen et. al. (1981) by using regression curves for R_n as function of cloud observations, global radiation or solar elevation. Meteorological data on wind speed and temperature at screen height are also used. In the Holtslag and van Ulden heat flux method R_n is also calculated using regression curves but as function of total cloud cover, the temperature at screen height and solar elevation.

The latent heat flux is described by the Penman-Monteith equation

$$Q_E = \frac{(R_n - Q_G) r_a (\Delta/\gamma_p) + Dq \rho c_p / \gamma_p}{r_s + (1+(\Delta/\gamma_p)) r_a} \qquad (2.2.2)$$

where Δ is the gradient of the saturated vapour pressure with respect to temperature, γ_p is the psychrometric constant, Dq is the humidity deficit in air,

$$Dq = e_s(T) - e \qquad (2.2.3)$$

where $e_s(T)$ is the saturated vapour pressure at the temperature T, e is the actual vapour pressure, r_a is the aerodynamic resistance and r_s is the surface resistance.

In the Berkowicz and Prahm heat flux method the aerodynamic resistance is expressed in terms of known flux profile relationships based on Monin-Obukhov's similarity theory. The surface resistance is related to the humidity deficit in the air, Dq, by the following equation

$$r_s = (Dq / F)(\rho c_p / \gamma_p) \qquad (2.2.4)$$

where F is an empirical function of the surface moisture conditions and is depending on net radiation and accumulated net radiation since last precipitation. The soil heat flux is modelled as a certain fraction of the sensible heat flux

$$Q_G = \alpha_g H \qquad (2.2.5)$$

where α_g is a constant with a typical value of 0.3 for a grass covered surface. The sensible heat flux can now be derived from equations (2.2.1), (2.2.2) and (2.2.5)

$$H = \frac{R_n(r_S + r_a) - Dq(\rho c_p / \gamma_p)}{r_S + (1+\Delta/\gamma_p) r_a + \alpha_g (r_a + r_S)} \qquad (2.2.6)$$

which is the basic equation for the Berkowicz and Prahm heat flux method.

To avoid the difficult problem with the surface resistance Holtslag and van Ulden (1983) simplified the Penman-Monteith equation in such a way that the surface resistance and the aerodynamic resistance are not explicitly described. The sensible heat flux is calculated by the following equation:

$$H = \frac{(1-a_s)+(\gamma/s')}{1+(\gamma/s')}(R_n - Q_G) - \beta_s \qquad (2.2.7)$$

where $s' = dq_s/dT$ with q_s being the saturated specific humidity and $\gamma = c_p/\lambda$ where c_p is the specific heat of air at constant pressure and λ the latent heat of water vaporization

The parameters α_s and β_s are empirical and are thought to vary with different soil moisture conditions. For moist grass covered surfaces $\alpha_s \approx 1$ and $\beta_s \approx 20$ Wm^{-2} were found to be good estimates. The soil heat flux, Q_G , is calculated as a factor of the net radiation. According to (De Bruin and Holtslag, 1982) a good estimate for Q_G is

$$Q_G = c_G R_n \qquad (2.2.8)$$

where c_G = 0.1 is obtained for a grass covered surface for daytime in the Netherlands. With these values, equation (2.2.7) can be simplified for daytime conditions (and for a temperature of 15°C) to:

$$H = 0.34(R_n - 58) \qquad (2.2.9)$$

The modelling of the Priestley-Taylor parameter in the HU-scheme is described in detail in Holtslag (1987). The parameter α_s is a function of the surface moisture. α_s is evaluated in the FMI -model according to table 2.2.1:

Table 2.2.1: Values of Priestley-Taylor parameter α_s in the FMI -model

α_s	synoptic measurements
1.0	night-time OR (S_U >4 or S_U =2) OR (49<W_W <100)
0.9	19<W_W<30 AND none of the above holds
0.8	4<W_2<10 AND none of the above holds
0.7	4<W_1<10 AND none of the above holds
0.6	rr>5.0 AND none of the above holds
0.5	none of the above holds

where rr is the precipitation of the last 12 hours (mm), S_U is the synoptic code for the state of the ground, W_W, W_1 and W_2 are synoptic codes for the present weather, weather of the previous hour and weather of the previous 3 hours, correspondingly.

The Holtslag and van Ulden heat flux method is a combination of schemes by Holtslag and van Ulden (1983) for daytime and by Holtslag and van Ulden (1982) for the night.

The two heat flux methods described above are widely used in different meteorological preprocessor models for dispersion calculations. The Finnish Meteorological Institute has based its preprocessor model on the method of Holtslag and van Ulden with some modifications (Karppinen et. al.,1996). The preprocessor models used in Denmark and Sweden are based on the method of Berkowicz and Prahm (Olesen and Brown,1992 and Omstedt, 1988). The relationship between these two basic schemes (HU,BP) and other commonly used preprocessors is shown in Fig. 2.2.1.

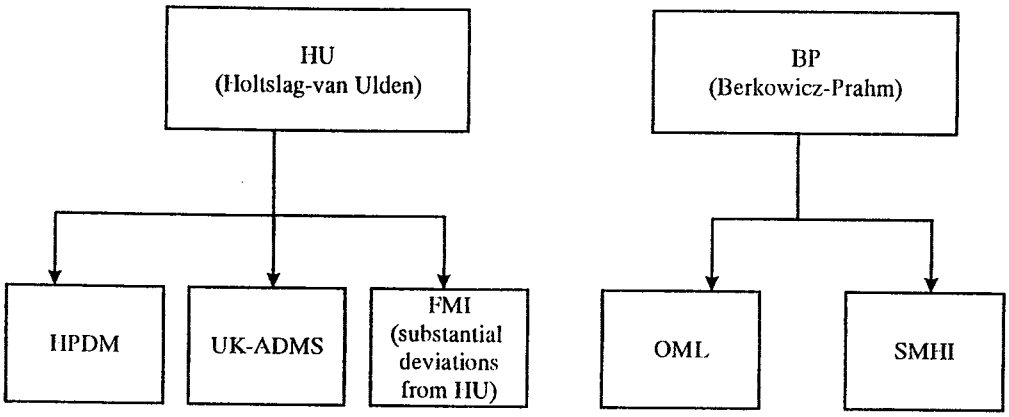

Fig. 2.2.1: Family tree showing the relationship between the preprocessors discussed in the report. See the explanation below for details.

Explanation to the family tree

Holtslag-van Ulden scheme:

This is one of the two basic schemes. As opposed to the BP scheme, it makes use of the Priestly-Taylor parameter α_s which must be prescribed.

Berkowicz-Prahm scheme:

This is the other basic scheme. It attempts to account for surface moisture by keeping track of the history of rainfall events. It avoids use of the α_s parameter, but the surface resistance r_s must be known (an empirical function is used for this purpose).

HPDM:

This preprocessor is not discussed in any detail in the present report. The HPDM preprocessor described by Hanna and Chang (1992) is based on the Holtslag-van Ulden scheme, but various constants are changed in order to account for urban conditions.

UK-ADMS:

This preprocessor is not discussed in any detail in the present report. The UK-ADMS preprocessor is based on the Holtslag-van Ulden scheme and is described by e.g.. Carruthers et al., 1994.

FMI:

In the original Holtslag-van Ulden scheme the user is required to prescribe a value of the Priestly-Taylor parameter, α_s. However, α_s is not constant, but depends on recent rainfall etc.. In view of this difficulty, the FMI scheme includes a procedure for estimation of α_s based on synoptic weather conditions and rainfall.

The FMI scheme attemps to improve the estimation of net radiation by using hourly sunshine duration data as an input parameter. In case sunshine data are not available, a default method based on cloud observations is used. The HU scheme was modified, as at high latitudes net radiation correlates better with sunshine duration than with cloud cover observations. Cloud cover observations may lead to erroneous net radiation estimates.

The longwave radiation from clouds is modelled by another regression equation, which uses the total cloudiness and cloud height as explaining parameters. All the regression coefficent estimates are based on Finnish observation data.

OML:

OML is the original computer implementation of the Berkowicz-Prahm scheme as it was developed by the group of Berkowicz and Prahm at NERI, Denmark. The implementation is documented in a report by Olesen and Brown (1992).

SMHI:

The SMHI scheme is an implementation of the Berkowicz-Prahm scheme which is very close to OML.

In chapter 4, results from a comparison between the preprocessor models used at the Finnish Meteorological Institute (the FMI-model) and at the Swedish Meteorological and Hydrological Institute (the SMHI-model) are shown.

2.3 PARAMETERIZATION OF THE GROUND HEAT FLUX

The primary transport process in the soil is molecular conduction. This allows the ground (or soil) heat flux to be calculated from the temperature gradient and the thermal conductivity appropriate for the depth and soil type. It can be inferred from the second law of thermodynamics that, when sources or sinks of heat within the soil are absent, the difference between the ground heat flux at the surface Q_G and the flux at a depth z, Q_{Gz} varies with the change in heat storage within the layer. This is given by the average time rate of change in soil temperature and can be written as the following relation

$$Q_G - Q_{Gz} = -C_g \frac{\partial T}{\partial t} dz \qquad (2.3.1)$$

where Cg is the volumetric heat capacity.
The ground heat flux Q_G is small when compared to the other three flux components of the energy balance (net radiation R_n, sensible heat flux H, latent heat flux Q_E) near the earth's surface, yet not insignificant. Mayocchi (1995) showed that neglecting heat storage and latent heat transfer in it's parametrization can bring in errors as large as 80 W/m^2 and 28 W/m^2, respectively. Latent heat transfer was often omitted in the soil analyses.

2.3.1 The measurements

The ground heat flux is derived from measurements made with ground heat flux plates. The ground heat flux should ideally be measured directly at the surface. Technical problems and modifications of the near-surface conditions occur however when a heat flux plate is buried very close to the surface. On the other hand, the deeper the plate is placed in the soil, the less it reflects the actual surface heat flux. A correction, based on the temperature gradient in the soil, is then required to account for the heat storage which occurs in the layer above the plate.
Fig. 2.3.1 presents a three-day time series of the ground heat flux measured by three plates at a depth of 8 cm separated horizontally by 50 cm (Muehlemann, 1996). It shows a better spatial homogeneity of the heat flux under wet soil conditions (in this case after a short, but intense rainfall). Possibly, the water also homogenized the soil conditions at proximity of the plates.

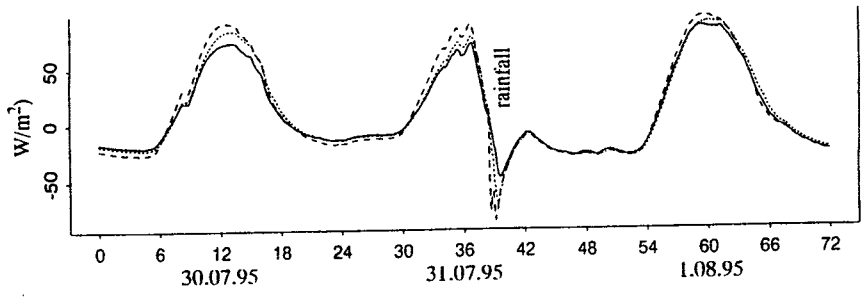

Figure 2.3.1: Measured ground heat flux from three heat flux plates, installed at 8 cm depth

The heat soil capacity C_g in equation (2.3.1) is defined as the sum of the specific heat capacities of the soil constituents: minerals, organic components, water and air. A soil analysis will give the volume fractions (in %) for the three major constituents (the heat capacity of air can be neglected). The calculation of C_g occurs then with standard values for the specific heat capacities. Heat soil capacities measured under wet and dry conditions gave differences between mean values up to 3.6 %, which produces an error in the surface heat flux of about 3 %.

2.3.2 The models

The need to parameterize the ground heat flux arises from the lack of measurements and the poor knowledge of this quantity. Simple schemes can be deduced from the following consideration: ground heating during the day is nearly balanced by cooling at night, thus, the heat budget in the soil remains weak over a whole day. Some general circulation models therefore assume that $Q_G=0$.

Proportionality model

Two simple possibilities are to assume a proportionality between the ground heat flux and either the net radiation R_n or the atmospheric turbulent heat flux H.

$$Q_G = c_G \cdot R_n \quad \text{or} \quad Q_G = \alpha g \cdot H \tag{2.3.2}$$

where the value $c_G = 0.1 \pm 0.05$ was obtained during clear daytime for a grass covered surface (Holtslag and van Ulden, 1983). Stull (1989) proposed a value of $c_G = 0.5$ for night-time conditions. Increasing soil dryness increases the relative contribution of the net radiation flux converted into sensible heat flux, because less energy is going to evaporation. Berkowicz (1982) therefore proposed a relationship between the ground heat flux and the sensible heat flux. The proportionality parameter α_g depends on the actual conductivity of the soil and the value 0.3 is often proposed for both night- and daytime.

Method of Holtslag and van Ulden (1983 & 1985)

The high resistance and low heat capacity of both air and vegetation justify the assumption of a strong correlation between the ground heat flux and the temperature difference (T_r-T_o) between the surface (o) and a reference level (r) in the air.

$$Q_G = -A_G(T_r - T_0) = \left(A_G / 4\pi T_r^3\right) C_s R_n \tag{2.3.3}$$

where A_G is an empirical coefficient for the ground heat transfer. It has been estimated to 5 $Wm^{-2}K^{-1}$ for a grass surface. The reference level (r) should be chosen above the layer which exhibits strong temperature gradients. Van Ulden and Holtslag found 50 m to be a suitable height. The parameterization of (T_r-T_o) differs for day and night. During the day, it is strongly

correlated with the net radiation R_n, related through the surface heating coefficient C_s, which may vary with the surface moisture. At night, (T_r-T_o) is strongly affected by the wind speed. In the latter case, surface layer similarity theory is used.

Arya's model

The model of Arya (1988) uses the solution of Fourier's heat conduction equation (2.4.7). It can be applied to both diurnal and annual temperature waves through the soil (considered as a homogeneous medium). The model further assumes that thermal diffusivity remains constant over the whole period and that the surface temperature follows a nearly sinusoidal perturbation. The latter condition is restrictive for the simulation of the diurnal variation.

Force-Restore Method

The method explained by Stull (1989) is based upon the assumption that the heat flux from deep soil tends to restore the surface slab temperature, thereby opposing radiative forcing. Based upon equation (2.3.1) and the relation of the energy balance and neglecting the latent heat flux, the ground heat flux is found to satisfy:

$$-Q_G = C_G \frac{\partial T_G}{\partial t} + 2\pi \frac{C_G}{P}(T_G - T_m) \qquad (2.3.4)$$

when P is a time period (daily circle).

The major part of soil temperature changes occurs within a shallow layer near the surface. A two-layer model captures the essence of heat transfer in the soil by superposing a shallow slab of soil, of thickness d_s and temperature T_G, bounded below by a thick slab which has an constant averaged temperature T_m. The amplitude of the thermal wave decrease exponentially with the depth so that at $z = d_s$ the wave amplitude is reduced to about 37%. of the value at the surface. $\rho \cdot c = C_g d_s$ is the heat capacity per unit area for the considered slab of soil of thickness d_s, soil density ρ and specific heat c.

2.4 SURFACE ENERGY BALANCE MODELS

2.4.1 Premises

Surface energy balance models generally deal with the evaluation of the all-wave radiation budget or net radiation R_n at the earth's surface and its partioning into convective fluxes to or from the atmosphere together with conduction to or from the underlying soil.

Contributions to the net radiation are the incoming short-wave or global radiation $K\downarrow$, the outgoing short-wave radiation $K\uparrow$, the incoming long-wave radiation $L\downarrow$, and the outgoing long-wave radiation $L\uparrow$.

The basic formula is:

$$R_n = K\downarrow + K\uparrow + L\downarrow + L\uparrow \qquad (2.4.1)$$

$K\downarrow$ and $K\uparrow$ may be summarized as K^*, the net short-wave radiation, and analogous $L\downarrow$ and $L\uparrow$ may be summarized as L^*, the net long-wave radiation:

$$K^* = K\downarrow + K\uparrow \quad \text{and} \quad L^* = L\downarrow + L\uparrow \qquad (2.4.2)$$

So $$R_n = K^* + L^* \qquad (2.4.3)$$

The net radiation R_n is the basic input to the surface energy balance. The radiative surplus or deficit, in most cases evidently connected with day or night time respectively, is partitioned between the sensible heat flux H, the latent heat flux Q_E, and the ground heat flux Q_G (see equation (2.1)).

An extra storage term, which is sometimes taken into account when treating complex surface layers, e.g. as in cities, is not considered here.

2.4.2 Some types of energy balance models

Simple energy balance models deal with the evaluation of the components of equation (2.1) for a given location in horizontally homogeneous conditions without advective energy fluxes.

The net radiation in those models is

- assumed to be known
  - . by measurements
  - . as output from radiation models

or

- calculated from formulae like

$$R_n = (1-A)\, K\downarrow + L\downarrow - \varepsilon\, \sigma\, T_0^4 \qquad (2.4.4)$$

with empirical parameterizations and/or otherwise known values of $K\downarrow$ and $L\downarrow$, albedo A, emissivity ε, and surface temperature T_0.

The sensible heat flux H is estimated through the profile method based on measurements of wind speed and potential temperature at two different heights in the surface layer of the atmosphere, where the fluxes are assumed to be constant with height.

The latent heat flux Q_E is evaluated either by analogy to H with the profile method or under the condition, that the Bowen's ratio Bo is known and valid:

$$Q_E = Bo\ H \tag{2.4.5}$$

The ground heat flux Q_G may be calculated from

$$Q_G = \lambda_{so} \left(\frac{\partial T_s}{\partial z}\right)_0 \tag{2.4.6}$$

in connection with a numerical solution of the unstationary equation for the subsoil temperature T_s

$$\frac{\partial T_s}{\partial t} = \frac{\lambda_s}{\rho_s\ c_s}\left(\frac{\partial^2 T_s}{\partial z^2}\right)_0 \tag{2.4.7}$$

Where λ_s is the thermal conductivity of the soil, ρ_s the soil density and c_s, the specific heat capacity of the soil.

Examples of such models are those from Myrup (1969), Kerschgens (1987), and Stathers (1988). The models differ in their needs for input data and parameterization of physical processes. More sophisticated models take into account complex topography and stomata processes like the one of Todhunter (1988).

Another refined numerical procedure to calculate energy fluxes at the surface was developed by Blackadar (1979). Under the guidance of Kerschgens the Blackadar model was modified by Roos (1995) and named EBiMo (Energie-Bilanz-Modell). The goal of the effort was to obtain a practical tool for statistical evaluations in connection with studies on local climate changes, e.g. for estimating the anthropogenic influence on the energy balance components by changes in land use.

EBiMo is an example of a 1-dimensional model of the planetary boundary layer with a vertical extension up to about 3 km above the surface and coupled with a soil model including vegetation. For input, radiosonde data are needed as well as surface based meteorological observations and soil specific information including vegetational indices.

The output list comprises the following results in two minutes time resolution:

- date and time
- surface temperature
- temperature of vegetation
- air temperature 5 m agl
- dew point 5 m agl
- surface sensible heat flux H
- surface latent heat flux Q_E
- surface net short-wave radiation K^*
- surface net long-wave radiation L^*
- surface net radiation R_n
- ground heat flux Q_G
- short-wave irradiance at the surface $K\downarrow$

The program is written in Fortran 77 and available (see chapter 10).

2.4.3 Complex mesoscale models

For the last 20 years, complex 3-dimensional models have been developed for various applications. They are based on the prognostic equations for atmospheric flow in non-hydrostatic conditions.

These models are working in areas with an extension of about 100 km to 1 km. Typical applications are the simulation of the diurnal wind regime in valleys and also the problem of cold air flow during night time in smooth shaped landscape. These models necessarily have to deal with the energy fluxes at or near the surface. They all use a wide variety of parameterizations and approximations. Their output contains a lot of information that can be used further in dispersion models. Especially, Lagrangian particle models make use of the results of non-hydrostatic meteorological models as input data.

A list of currently used non-hydrostatic models for climatological purposes within the above mentioned scale is given by Schlünzen (1994), together with some characteristic features of each model.

2.5 OUTPUT OF NUMERICAL WEATHER PREDICTION MODELS

Operational numerical weather prediction (NWP) models provide, besides other information, data of the surface energy balance and its components on different scales. At present, NWP models are working from the global scale down to regional scales with horizontal resolutions of about 10 km and vertical resolutions of about 20 levels or more from the surface up to 50 hPa or higher.

The atmospheric boundary layer is represented by several levels in such a way, that it is possible to determine the turbulent fluxes of sensible heat and of latent heat at the surface. The parameterization of radiation processes within NWP models allows the calculation of the components of the net radiation at the surface. Most NWP models include a multi-layer soil submodel enabling the determination of the ground heat flux. Results of an international comparsion of global NWP models concerning the components of the surface energy budget are given in Annex A.

Another comparsion has been carried out by Wotawa et. al. (1996) between results of the meteorological preprocessor OML (Olesen and Brown, 1988) and evaluations of ECMWF's NWP model. The comparsion shows systematic differences, especially for the friction velocities, and also stochastic deviations and great uncertainties concerning other parameters.

The Europe-Model (EM) of Deutscher Wetterdienst, covering Europe and a part of the North Atlantic Ocean, is an example of NWP models, as they similarly are run also by other national weather services. A short description of the model and its output concerning surface energy balance is given in Annex A.

The scientific development on NWP models is going on as well as computer capacity is growing rapidly. Therfore, it will be possible in the near future to run non-hydrostatic NWP models operationally with horizontal resolutions below 10 km and 40 or more vertical levels. So, the results of such models will become more and more interesting for the determination of the surface energy balance.

3. DATA SETS

3.1 INPUT DATA FOR EACH OF THE METHODS AND MODELS

3.1.1 Input data for the profile method

Use of the profile method requires knowledge of differences of wind, temperature and humidity at two different levels in the surface boundary layer.
The accuracy of the method is better when the distance between the two measurement levels is large.
One should notice that, for the analytical solution, wind, temperature and humindity have to be given at the same levels.

3.1.2 Input data for the resistance method

Standard routine meteorological data is used such as wind speed (u), temperature (T), dewpoint temperature (T_d), cloud observations (N_{tot},N_l,N_m,N_h)and precipitation. A comparison between input data used by the Berkowicz and Prahm heat flux method (BP) and the Holtslag and van Ulden heat flux method (HU) is given in the following two tables. In the FMI-model also hourly relative sunshine time is used.

Table 3.1.1 Calculated parameters using the Berkowicz and Prahm heat flux method (BP) and their dependence on meteorological data and other calculated surface parameters.

	BP	
Parameter	Input data needed	Surface parameter needed
R_n	N_{tot}, N_l, N_m, N_h u, T	
r_s	T_d, T, *precipitation*	R_n
r_a	u, z_0	L_*, u_*
H	T, T_d	R_n, r_s, r_a
u_*	u, z_0	L_*
L_*	T	u_*, H

Table 3.1.2 Calculated parameters using the Holtslag and van Ulden heat flux method (HU) and their dependence on meteorological data and other calculated surface parameters.

	HU	
Parameter	Input data needed	Surface parameter needed
R_n	N_{tot}, T	
α_s, β_s	*precipitation*	
H	T	R_n, α_s, β_s
u_*	u, z_0	L_*
L_*	T	u_*, H

3.1.3 Input data for surface energy balance models

The input data needed are partly mentioned in 2.4. For a detailed description, the references given in connection with the models can be used.

3.1.4 Input data for NWP models

Input data for operational NWP models originate mainly from synoptic stations (surface observations, radiosonde measurements), satellites and aircraft. They are checked and assimilated with respect to the model grid and the starting time of the prognosis. The initialization procedure takes care to harmonize the numerical analysis with the difference equations used for the time integration.

A more detailed description with respect to the example of the above mentioned model EM is given in Annex A.

The assimilated and initialized numerical analyses of the NWP models, when archived and available, will become more and more of great value for environmental purposes including the application of dispersion models, when taking into account the following aspects:
- building of climatologically usable time series
- development of operational non-hydrostatic NWP models, necessarily working on relatively high resolved grids, so there will be a convergence of the results with the outcome of complex mesoscale models for local climatological purposes.

3.2 SATELLITE DATA

The radiation measurements from polar orbiting satellites (e.g. the NOAA series) as well as those from geostationary satellites (like METEOSAT) are used to derive meteorological data. They may serve as input to numerical methods (including models) or for evaluation purposes. Among them are a lot of products, that are of great interest in connection with the energy balance at the earth surface (WMO, 1995). Satellite data comprise

- land surface (soil) temperature
- sea surface temperature
- cloud parameters, e.g.
  - cloud cover in different heights
  - cloud types including fog
- precipitation
- soil moisture
- global radiation, equivalent to the incomingshort-wave radiation
- absorbed short-wave radiation
- long-wave radiation
- surface albedo
- vegetation index
- land use

Additionally, the latent heat flux may be calculated from satellite measurements (Schulz et. al., 1995).

Polar orbiting satellites have the advantage of giving information in a high spatial resolution (1,1 km concerning meteorological parameters; 30 m concerning Landsat data) in a moving, but limited strip Geostationary satellites have the advantage of covering a large area at the same time, but with less horizontal resolution (5 km in the visual and 8 km in the infrared range over Europe).

In some meteorological services, these parameters are already extracted operationally. E.g. in Deutscher Wetterdienst, the global radiation at the surface is derived from Meteosat images in the visible range. The global radiation is evaluated as a daily mean value in a horizontal grid of 8km covering central Europe. Figs. 3.2.1 and 3.2.2 show comparisons of satellite derived daily sums of global radiation with ground based measurements.

The European Agency EUMETSAT is considering to support the establishment of Satellite application facilities (SAFs) with the aim to focus the European efforts in extracting and using meteorological (among other environmental) information from satellite data. Plans include the establishment of SAFs on 'Nowcasting', 'Ocean and sea ice', 'Ozone', 'Climate monitoring', and 'Numerical weather prediction'.

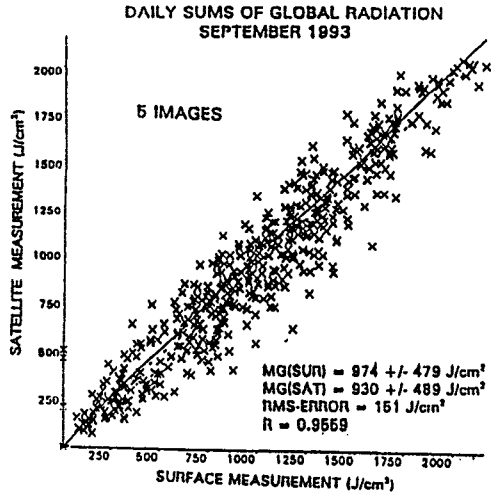

Fig. 3.2.1 Comparison of satellite derived daily sums of global radiation with ground based measurements. The results are based on 5 images per day.

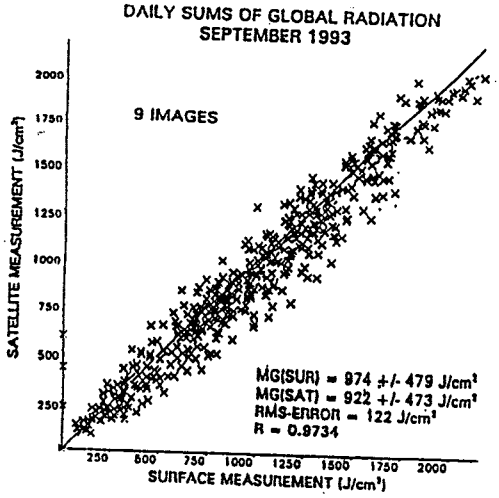

Fig. 3.2.2 Comparison of satellite derived daily sums of global radiation with ground based measurements. The results are based on 9 images per day.

4. INTERCOMPARISON STUDIES

4.1 EARLIER WORK

The two different resistance methods that were discussed in section 2.4 have earlier been compared with experimental data. The Berkowicz and Prahm heat flux method (1982) was developed using experimental data from Højbakkegaard in Denmark, Marsta in Sweden and Cabauw in the Netherlands. The Holtslag and van Ulden heat flux method (1982,1983) was developed using mainly data from Cabauw in the Netherlands. All these data cover a broad range of weather conditions, but only for grass-covered surfaces.

Recently Galinski and Thomson (1995) compared the sensible heat flux from these two methods and a third one (Smith, 1990) with almost 3 years of measurements from Cardington in UK. Their general conclusion is that the results from all three preprocessors show useful correlation with measured heat fluxes during daytime (neutral or unstable conditions), although the spread is quite large. During night-time (stable conditions) the correlation between calculations and measurements are worse for all three preprocessors. When comparing the three schemes with each other, their conclusion is that the Berkowicz and Prahm heat flux method performed best during daytime conditions while the Holtslag and van Ulden heat flux method performed best during night-time.

4.2 INTERCOMPARSION OF METHODS

In one study under COST 710, the FMI and the SMHI preprocessors were intercompared. The schemes are based on two widely used preprocessing methods:

1. the FMI scheme which is based on the van Ulden-Holtslag scheme (HU) (van Ulden and Holtslag, 1985), but deviates from it in certain respects.
2. the SMHI scheme which is based on the Berkowicz-Prahm scheme (BP) (Berkowicz and Prahm, 1982b), and fully represents the properties of the scheme. (For a part of the study the implementation of the BP scheme was that of the Danish OML meteorological preprocessor.)

The study aimed to investigate the properties of the two schemes relative to each other, and did not involve direct comparisons with observations.
In the following, the differences between the parametrizations of individual terms of the surface energy balance equation are investigated. Furthermore, on the basis of identical input data (one year of data from southern Finland), the output of the two schemes is compared.

4.2.1 Comparison between the parametrization of individual terms

Net radiation estimates

Both methods use regression methods to estimate the total net radiation R_N. The used predictors in the regression equations are different. Also the data on which the regression coefficients are based are from different stations and different periods of time.

The HU-method divides the net radiation into three parts: the shortwave radiation from the sun, blackbody radiation from clouds and the ground, and the longwave radiation of the atmosphere. The shortwave radiation is approximated in the FMI scheme by a regression equation which uses observed hourly sunshine time as the regression model variable. The radiation from clouds is modelled by another regression equation, which uses the total cloudiness and cloud height as explaining parameters.

The BP-method uses two regression models (one for daytime and one for night-time) which use the synoptic measurements of cloudiness as the most important explanatory variables.

The net radiation estimates of these two schemes are illustrated in figure 4.2.1.

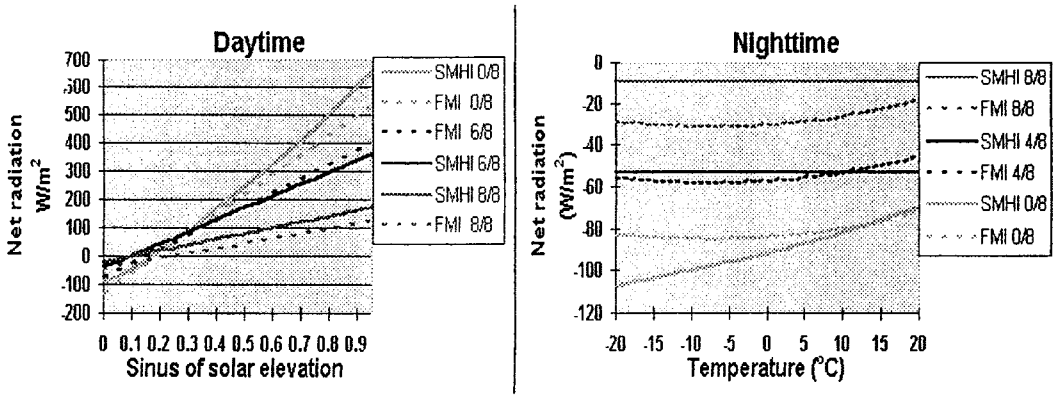

Fig.4.2.1. Net radiation estimates by FMI (HU-based)- and SMHI (BP-based) preprocessor models as function of solar elevation, temperature and cloudiness (in octas)

There is a noticeable difference between the net radiation according to the two schemes. Under daytime clear sky conditions the difference increases as solar elevation increases. Under clear night-time conditions the difference increases as temperature decreases. The difference in the clear-sky night-time estimations of net radiation comes directly from the temperature dependence in the regression equations. In the BP-method (SMHI) the dependence of net radiation on temperature is simply: $R_n \sim T^6$, which means that R_n decreases monotonically with temperature. In the FMI-scheme the dominant part of the net radiation depends on temperature as: $R_n \sim cT^6\text{-}T^4$. This function has an absolute minimum at the temperature $T \approx -6$ °C. Although the additional terms affect the location of the absolute minima, the behaviour of the net radiation as a function of temperature remains similar as illustrated in figure 4.2.1.

Partitioning the energy

The partitioning of the energy to latent (Q_E) and sensible (H) heat fluxes is based on the Penman-Monteith approach (Monteith, 1981).

The two methods have one basic difference in their energy partitioning scheme. While the Berkowicz/Prahm-scheme evaluates the resistances r_a and r_c and the humidity deficit in a quite complicated way, the HU-scheme utilises the modified Priestley-Taylor model which divides the evaporation in one part which is strongly correlated to the difference of net radiation and ground heat flux (R_n-Q_G) and another part which is not. Therefore, in the HU-scheme only two empirical parameters (α_S and β_S) therefore have to be evaluated.

The surface and soil moisture are estimated differently in the models. The FMI-model (modified HU) uses synoptic weather codes and rain amount to estimate the surface moisture and the modified Priestly-Taylor parameter α_S. The Berkowicz/Prahm-model uses the

accumulated net radiation for the measure of the soil moisture. These estimates are not directly comparable since the partition schemes and the use of these moisture estimates differs in the models.

Solving the system of equations

The profile equations used by these two methods are based on different approximations of the universal functions Ψ_m and Ψ_h. However, both approximations are based on the same original work of Businger et al. (1971), so there are no significant differences in the profile equations used by these two methods. The final determination of the meteorological parameters (turbulence length-scales: MO-length L_*, friction velocity u_*, temperature scale Θ_*) is performed in both models using the same sets of equations and basically the same kind of profile equations.

4.2.2 Statistical comparison of the output of the two models

As the two methods differ quite a lot in the details of their parametrization, it is extremely difficult to compare the models without actually performing some calculations with the models using identical synoptic data for the input of the two models.

The part of the study described in the following was not based on the SMHI implementation of the BP-scheme, but on the original implementation of the scheme in the OML preprocessor from the Danish National Environmental Research Institute (Olesen and Brown, 1992). However, the two implementations are very close to each other and can be assumed to fully represent the BP-scheme.

The results presented here cover one year of meteorological data, collected from southern Finland. The only preparation made before using the synoptic data as input to the preprocessors was an interpolation from 3 hour measurements to hourly values.

The quantile-quantile distribution of net radiation as estimated by the OML and FMI models are shown in Fig. 4.4.2. We observe that the distributions are very similar, except for a slight difference for net radiation values on the range 200-400 W/m^2. This small difference arises from the differences in the daytime net radiation estimates (Fig. 4.2.1.). In clear-sky situation the net radiation estimates of the OML-method are higher than the estimates of the FMI-method but as cloudiness increases the FMI-method starts to give higher estimates of net radiation than the OML-method.

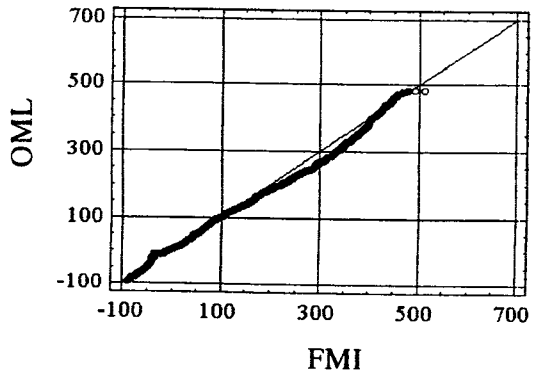

Fig. 4.2.2 Quantile-quantile plot of net radiation (R_N) in W/ m^2, estimates by the FMI (HU-based) and OML (BP-based) schemes.

This figure suggests strongly that in practice (in a statistical sense) the estimates of net radiation by these two models give very similar results.

The plot of the cumulative distributions of sensible heat flux estimates of these two models is presented in figure 4.2.3, which shows that the energy partitioning schemes compared differ quite a lot, not only in the parametrisation details but also in the resulting sensible heat flux estimates.

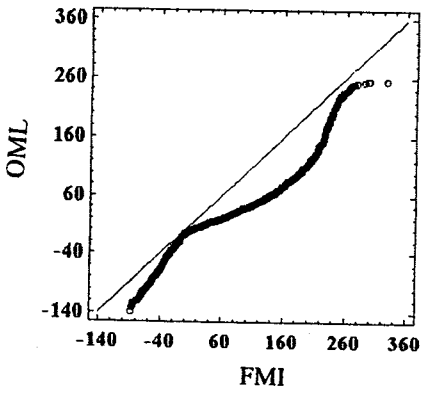

Fig. 4.2.3. Quantile-quantile plot of estimates of sensible heat flux H in W/m^2.

There is one similarity in the estimates: the ratio of number of stable vs. number of unstable situations is roughly equal for these two models. On the stable side the OML-model (BP) gives consistently more negative heat flux values than the FMI-model (HU). On the unstable side the FMI-model gives larger sensible heat flux values than the OML-model. This suggests that these two parametrisation schemes divide differently the available energy between the latent and sensible heat fluxes although the basic input data are identical and the net radiation estimates are nearly identical.

The density distribution of the inverse MO-lengths produced by these two models is presented in Fig. 4.2.4.

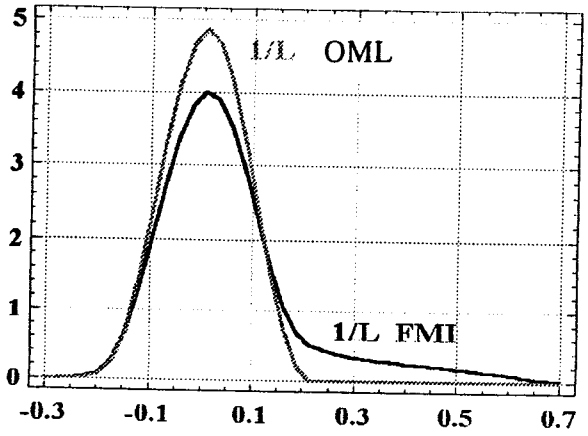

Fig. 4.2.4 Density distribution of the inverse Monin-Obukhov lengths (1/L*) in 1/m.

There is a clear difference between the two curves: the BP-model impedes the growth of 1/L* on the stable side, which makes the distribution function quite symmetrical around the neutral (1/L* small) area. There is not such a cut off in the Finnish model (HU), which can generate quite many "super-stable" situations. This is a very important difference for the air quality modeller as these very stable situations are often connected with air-pollution episodes. So it is important to be able to parameterise correctly these situations.

$$L_* = -\frac{u_*^3}{\kappa \frac{g}{T_0} \cdot \frac{H}{\rho c_p}} \qquad (4.3.1)$$

The net radiation (R_n) was also included in the comparison, since both schemes calculate it in order to estimate the sensible heat flux.

The data used for the comparisons were reduced to 1 hour averages. Since the synoptic data were available only for every third hour, these hours were used, although the preprocessors are capable of giving interpolated values for every hour. The measurements contained some unrealistically high sensible heat flux values and those data points were omitted from the analyses. The limits were set to -150 and 350 W/m^2 respectively, following Galinski and Thomson (1995). The omitted values were less than -500 W/m^2 or larger than 1000 W/m^2 which indicates that the analyses are not sensitive to the choice of limits. The reason for these unrealistic values have not been fully clarified yet, but they are believed to be caused by measurement errors. The preprocessor calculations were performed by SMHI and FMI respectively.

Results for the friction velocity (u_*) or momentum flux

Figure 4.3.1.1 shows comparisons between the measured values of u_* and those produced by the two preprocessors. As can be seen from the plots there is a fair agreement, although the spread is quite large. The correlation between measured and calculated values is about the same for the two preprocessors, but the FMI preprocessor (HU-based) tends to give higher u_*-values. The values calculated by the SMHI preprocessor (BP-based) agree quite well with the measurements over the whole range, but the values from the FMI scheme are on an average about 30% higher. This is also seen from the comparison between the two preprocessors in Figure 4.3.1.2, which, however, shows very high correlation between the two schemes. The main reason for the higher U_* values for the FMI scheme is the choice of surface roughness parameter, z_0. In the SMHI preprocessor z_0 is assumed to be equal to 1 cm if the surface is snow covered, while the FMI preprocessor assumes a value of 5 cm instead. With homogeneous snow covered ground, z_0 should be very small, but it should also reflect any inhomogeneities present.

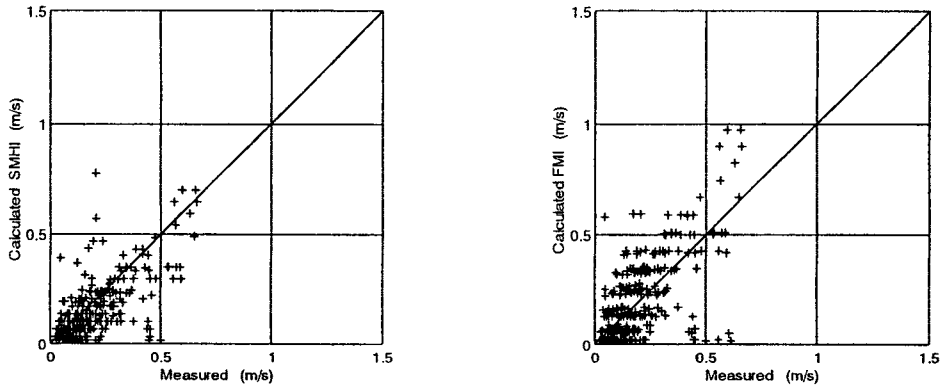

Figure 4.3.1.1. Measured values of friction velocity compared to calculated ones. The left panel shows the result for the SMHI (BP-based) meteorological preprocessor and the right panel those for FMI (HU-based).

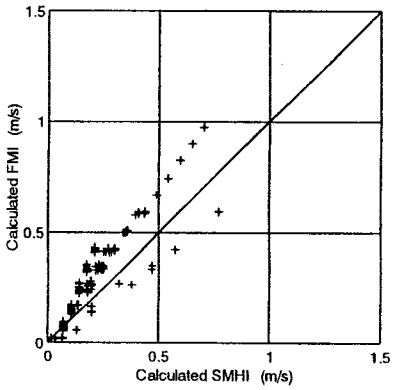

Figure 4.3.1.2. Comparison of the calculated friction velocity from the two preprocessors.

Results for the sensible heat flux and net radiation

The results for the sensible heat flux show much larger spread and the correlation is poor. In Figure 4.3.1.3 the comparisons between measured and calculated values are shown. In the following, the sensible heat flux is defined to be positive upwards and negative downwards, whereas the net radiation is positive downwards (towards the surface) and negative upwards. It deserves to be noted, that the measurements include some positive values of sensible heat flux while all the calculated values are negative. It should be mentioned that in conditions with low turbulence the direct measurements might not be representative, even though one-hour averages were used. This is because turbulence occurs intermittently when the wind speed is close to zero and there is a strong temperature inversion close to the ground. As can be seen from the plots, both preprocessors generally underestimate H, i.e. give lower sensible heat flux

than the measurements. When the measured values are close to zero the preprocessors estimate it to be somewhere in the range 0 to -70 W/m^2.

The comparison between the two preprocessors in Figure 4.3.1.4, also shows a large spread and that the correlation is poor. The general impression is that they disagree in most cases. If one of the preprocessors predicts a value close to 0, the other one seems to predict a large negative value and vice versa.

The fact that the preprocessors estimate H to be large and negative when the measurements show values close to 0 might be explained as the result of an underprediction of net radiation in such situations. Both preprocessors calculate the sensible heat flux by a surface energy balance method (for details see Karppinen et al., 1996) and the surface energy balance relies heavily on the estimated net radiation. The net radiation is parameterized using incoming short-wave radiation reduced for the effect of cloud amount and surface albedo, together with an estimate of incoming and outgoing long wave radiation. The conditions during this study were very special in this respect. The ground was covered by snow, i.e. the albedo was very high and the solar altitude was low, which increased the albedo even more. Furthermore, in situations with no short wave radiation, the net radiation is the balance between incoming and outgoing long wave radiation. The outgoing long wave radiation is proportional to the surface temperature, which means that it decreases with decreasing temperature. Thus, when the short wave radiation disappears, the radiation loss at the surface causes the surface temperature to decrease. When the temperature becomes low enough, the outgoing and incoming long wave radiation will balance out each other, and the temperature decrease will stop. This feature is not included in any of the preprocessors. Observations supporting this has been reported from another study in northern Sweden (Johansson et al., 1994) where measured values of the net radiation decreased with decreasing temperature to a certain limit, where it stopped. If the temperature then decreased further, the net radiation started to increase and finally, at the end of the night, it ended up close to 0.

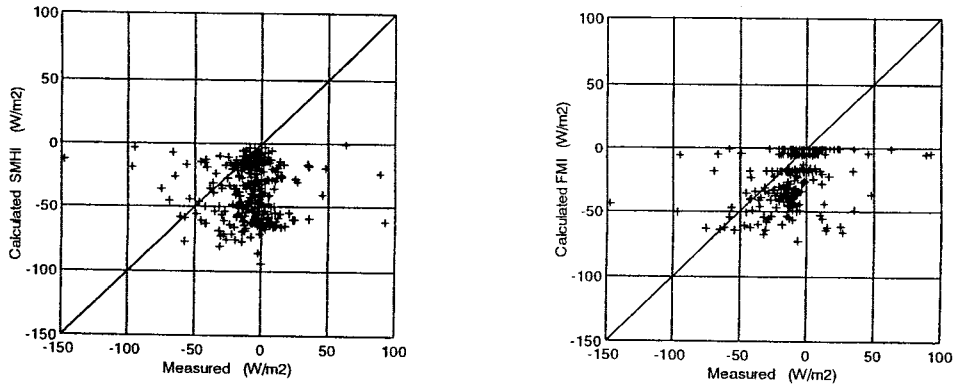

Figure 4.3.1.3. Measured values of sensible heat flux compared to calculated ones. The left panel shows the result for the SMHI meteorological preprocessor (BP-based) and the right panel those for FMI (HU-based).

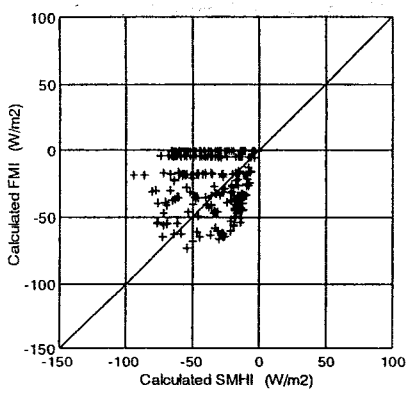

Figure 4.3.1.4. Comparison of the calculated sensible heat flux from the two preprocessors.

When studying this phenomenon it is helpful to look at the comparisons of net radiation, which are shown in Figure 4.3.1.5. The plots look in a way similar to those for the sensible heat flux. There is a number of measurements indicating positive net radiation (i.e. net incoming radiation) while the preprocessors almost always give negative values (i.e. net outgoing radiation). The calculated net radiation seems to become too large and negative during conditions when the measurements give values close to 0, this is most clearly shown for the SMHI preprocessor. These results indicate that the use of measured net radiation, as input to the preprocessors, could improve their estimate of sensible heat flux and thereby L_*. This conclusion is different from that reached by Galinski and Thomson (1995) who found that the use of measurements of net radiation did not improve estimates of heat flux. However, their study was performed under much different conditions, where there was a fair agreement between estimated and measured net radiation. The use of net radiation as input to the meteorological preprocessors would also introduce another disadvantage, since it is a parameter not routinely available.

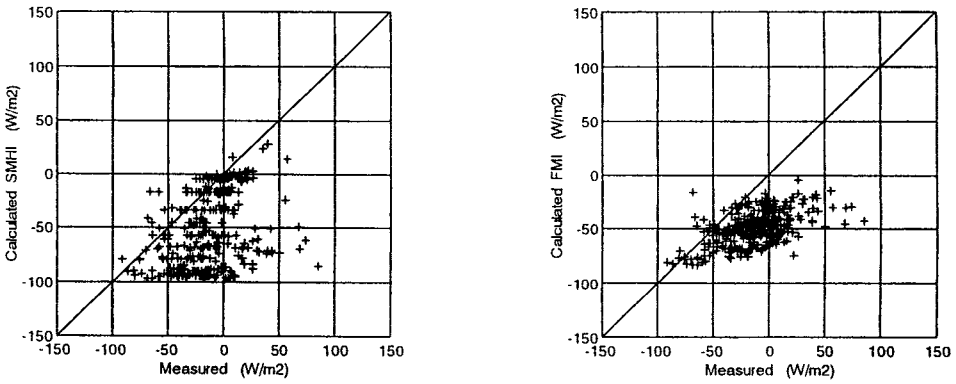

Figure 4.3.1.5. Measured values of net radiation compared to calculated ones. The left panel shows the result for the SMHI meteorological preprocessor (BP-based) and the right panel those for FMI (HU-based).

Results for the Monin-Obukhov length or stability classes

When estimating the dispersion parameters, the surface fluxes of heat and momentum are not used directly, instead they are combined into the Monin-Obukhov length, L_*. Comparing the values for L_* is not as easy as for the fluxes, since L_* is much more sensitive to small changes in either one of the surface fluxes. Plots similar to the ones for the fluxes above just show a lot of scatter. Instead the estimated L_*-values were translated into traditional Pasquill stability classes, following Golder (1972). The result is shown in Table 4.3.1.1.

According to the measurements about 15 % of the cases are in some of the unstable classes while the preprocessors only predict neutral or stable cases. This is in agreement with the earlier results for the comparison of H, where the measurements showed positive values but the preprocessors did not. Furthermore, it is seen that the SMHI scheme by far has the highest frequency of (very) stable cases. One explanation for this may be that the FMI scheme gives higher u_*-values than the SMHI one, and since larger values of u_* result in larger values of L_*, the classification becomes less stable.

Table 4.3.1.1. Relative distribution of the stability classes. The classification is based on measured surface fluxes (1 hour averages) or calculated surface fluxes from the two preprocessors (one value every 3:rd hour). The translation of the L_*-Values into Pasquill stability classes are according to Golder, 1972.

Pasquill class	Range in L_* (z_0=1 cm)	Relative frequency of observations (%)		
		Measurements	SMHI	FMI
B	$-17 < L_* < 0$	13	0	0
C	$-50 < L_* < -17$	4	0	0
D	$L_* < -50$ or $62 < L_*$	37	20	39
E	$14 < L_* < 62$	23	8	17
F	$0 < L_* < 14$	23	72	44

Discussion of results

This study has shown that in order to be used at high winter conditions the two tested meteorological preprocessors will have to be modified or further developed. The calculated friction velocities agreed fairly well with the measurements or at least showed a good correlation to them. The calculated heat fluxes, however, were lower than the measured values, and furthermore the disagreement between the two preprocessors was large. The poor correlation between observations and predictions indicates that some important parameters or physics are missing in the models. One reason for the disagreement between the calculated and measured heat fluxes may be that the parameterization of net radiation gives too low values. The calculated net radiation from the two preprocessors was also shown to differ from the measurements in a way similar to that of the heat flux. The reason for too low net radiation in the preprocessors may be the assumption of too high albedo value or the estimation of too high outgoing long wave radiation at very low temperatures. The albedo values assumed by the

preprocessors in this study are probably not too high, since the measurements are made above, and close to, a homogeneous snow surface. In reality, the albedo value used in meteorological preprocessors for dispersion models should be reduced from the values valid for homogeneous snow, because it should be representative for a much larger area. According to these findings the use of measured radiation may be supposed to improve the estimate of heat fluxes. The use of net radiation as input to the preprocessors will restrict their applicability, since net radiation is not routinely available from ordinary meteorological observation stations.

4.3.2 Intercomparison of the SMHI and FMI scheme for high-latitude spring and summer conditions

In this section, the two meteorological preprocessors from OML (SMHI) and FMI will be compared further. In the previous section, 4.3.1, the comparisons focused on the behaviour of the preprocessors under extreme winter conditions at high latitudes in northern Sweden. In the present section, these comparisons are extended with evaluations for spring and summer conditions at moderately high latitudes in central Sweden.

4.3.2.1 Field measurements

The measurement data were obtained from the international measurement campaign NOPEX (Northern Hemisphere Climate Processes Land-surface Experiment), where the overall objective is to quantify the energy and mass budgets for landscapes dominated by boreal forests. The NOPEX experiment region is situated in central Sweden in the surroundings of Uppsala (59°52'N,17°38'E). In general, this region is characterized by a flat landscape with a variation of the topography height between 30 and 70 meters above sea level. Vegetation types and ground usage consist of a mixture of boreal forests and agricultural regions. Even though forests as a whole are dominating this part of Sweden, areas are still found where major fractions of the ground are used for agricultural purposes. As for the NOPEX measurements, two concentrated field efforts have so far been performed, namely during 27 May - 23 June 1994 and 18 April - 14 July 1995.

The measurements used in this study are taken from both NOPEX field campaigns for two different sites. The first site is located at Marsta, about 10 km north of Uppsala, while the second one is found at Tisby, some 35 km west of Uppsala. These sites are situated in agricultural land-use regions, where the immediate site surroundings are covered with grass and herbs, while further away, fields covered with various kinds of crops are found.

Direct measurements were performed for the surface fluxes of heat and momentum, and for net radiation. At Marsta, the turbulent fluxes were measured at a height of 10 m, using a sonic anemometer (Solent Ultrasonic Anemometer 1012R2). Net radiation measurements were carried out with a Siemen-Ersking net radiometer mounted at a height of 1.5 m. The reference temperature was measured at 1.9 m above the ground. The Marsta data are given as 10-minute averages. At Tisby, the turbulent fluxes were measured at a height of 6.8 m using a sonic anemometer (Kaijo Denki DAT/TR-61B). The net radiation measurements were not available for the present study. The reference temperature at 2 m above the ground was measured only during the 1995 field campaign. The Tisby data are given as 30-minute averages. For the

purpose of comparing the measurements with the estimates from the preprocessors, the 10-minute averages from Marsta and the 30-minute averages from Tisby were both reduced to hourly averages.

The values for the friction velocity, surface sensible heat flux and Monin-Obukhov length were calculated as follows from the measurement data:

$$u_*^2 = \sqrt{\left(\overline{u'w'}\right)^2} \quad \text{or} \quad u_*^2 = \sqrt{\left(\overline{u'w'}\right)^2 + \left(\overline{v'w'}\right)^2}$$

$$H = c_p \rho \cdot \overline{w'T'}$$

$$L_* = - \frac{u_*^3}{\kappa \frac{g}{T_0} \frac{H}{c_p \rho}}$$

where u_* is the friction velocity, H the surface sensible heat flux, L_* the Monin-Obukhov length, u' and v' the turbulent deviations of horizontal momentum, w' the turbulent deviation of vertical momentum, T' the turbulent deviation of temperature, κ von Karman's constant (= 0.35), g the acceleration due to gravity (= 9.81 m/s^2), c_p the specific heat of dry air at constant pressure (= 1004.64 J/K/kg), ρ the density of dry air (= 1.29 kg/m^3), and T_0 the 2 m reference absolute temperature.

4.3.2.2 Synoptic observations and preprocessing

The meteorological preprocessors base their calculations completely upon regular synoptic observations (SYNOP). The synoptic station located most closely to Marsta and Tisby is Uppsala Airport, located in the northern part of the city of Uppsala. Marsta is located some 8 km north of the airport, and Tisby about 35 km west thereof. The synoptic parameters were first modified or prepared so as to provide the proper input format needed by the preprocessors. For the roughness length, a value of 0.02 m was used for all wind directions.

The FMI scheme requires one non-standard parameter that is not normally contained in SYNOP, namely the relative, hourly sunshine duration. This parameter is used as the regression variable for the estimation of the shortwave radiation component in the surface energy balance equation, see sections 2.4 and 4.2.1 for further details. Sunshine data were not available for the synoptic station at Uppsala Airport. For situations when this parameter is missing, the FMI scheme calculates the shortwave component by using a regression equation

which instead is a function of total cloud cover. The regression coefficients in this equation have been deduced from a 10-year measurement fit in Finland.

Using both preprocessors, calculations were performed for the standard synoptic observation periods at 0, 3, 6, 9, 12, 15, 18, and 21 GMT, giving values for the friction velocity, the surface sensible heat flux, net radiation and the Monin-Obukhov length. These values are then compared to the hourly averages of the field measurements at corresponding hours. The preprocessor calculations were made, utilizing computer codes provided by the Danish National Environmental Research Institute (OML) and the Finnish Meteorological Institute (FMI).

Snow was observed on scattered days during the month of April 1995, with four days of complete snow cover, and another four days where the ground is partially covered with snow.

4.3.2.3 Momentum flux

In Figure 4.3.2.1, comparisons of friction velocity are made between the two sites at Marsta and Tisby, as well as between the two meteorological preprocessors. The correlations between the measured and the calculated values in Figs. 4.3.2.1A-D are seen to roughly equal the correlation between the two measurements in Fig. 4.3.2.1F. This indicates that the estimates from the preprocessors are representative for the greater region around the synoptic station. However, the preprocessor estimates are slightly better correlated with the Marsta measurements, but this is natural in view of its closer location to the synoptic station. Fig. 4.3.2.1E shows that the results for the two preprocessors compare very well, yet the average values are about 30% higher for the FMI scheme. Moreover, the OML scheme appears to have difficulties in estimating low friction velocity values. In general these findings compare well with the results shown in figures 4.3.1.1 and 4.3.1.2 for high-latitude winter conditions.

4.3.2.4 Surface sensible heat flux

The results for the surface sensible heat flux show a somewhat lower correlation than for the friction velocity. In figure 4.3.2.2 the comparisons for the measured and computed values are shown. The heat flux is defined to be positive when directed upwards, and negative when directed downwards. As for the measurements, it is seen in Fig. 4.3.2.2F that the values for Marsta and Tisby correlate well. However, the average value of 46.8 W/m^2 at Tisby is higher than the 26.7 W/m^2 at Marsta.

The calculations by the OML preprocessor are in good agreement with the measurements, especially with those in Marsta, as shown in Fig. 4.3.2.2A, even though the average value of the OML estimates is some 20% lower than the measurements. In comparison with the Tisby measurements, the OML results tend on average to be even lower, especially for the higher positive fluxes, that is, for events with strong incoming solar radiation (Fig 4.3.2.2C). Apparently OML has difficulties in estimating sensible heat fluxes above 200 W/m^2.

The estimates provided by the FMI preprocessor split into two groupings (Figs. 4.3.2.2B and D). The first group consists of realistic surface flux calculations in the near-zero range of -50 W/m^2 to +50 W/m^2, corresponding to cases with low incoming solar radiation, e.g. nighttime cases or overcast skies. For this group the correlation is good. The second group is mostly made up of values larger than zero, corresponding to cases with higher incoming solar radiation values, e.g. daytime cases with low amounts of clouds. Here the estimates also have an upper cut-off value of about 100 W/m^2, and the correlation is very low, and actually close to zero.

For the FMI scheme, the probable cause for the differing behaviors between the two groups is the missing hourly sunshine data, which forces the model to use a regression based on total cloud cover data (see section 4.3.2.2). For cases with low incoming solar radiation, such as during nighttime or overcast skies, the incoming shortwave solar radiation component plays a minor role in the surface energy balance equation, and the missing sunshine information will not lead to critical errors. However, for cases with high solar radiation values, such as during daytime with relatively clear skies, the shortwave component in the surface energy balance equation plays a major role. The absence of sunshine data will then reduce the accuracy of the net radiation estimate, thus giving poor results for the sensible heat flux since it is strongly dependent upon the net radiation. These deviations can be seen in the comparison between the OML and FMI scheme in Fig. 4.3.2.2E.

The comparison between OML and FMI shows that the OML scheme underestimates the fluxes somewhat more than the FMI preprocessor for the case of near-zero fluxes. For this range of flux values, similar results are obtained in section 4.3.1 for the high-latitude winter conditions.

4.3.2.5 Net radiation

In Figure 4.3.2.3 the results for net radiation are shown. Here positive values imply a net incoming radiation, and negative values a net outgoing radiation. Measurements were made available only for the Marsta site, thus no results can be presented for Tisby. The figures show

very identical structures to those for the surface sensible heat flux in Fig. 4.3.2.2, which is reasonable, since the heat flux is a function of net radiation.

For the OML preprocessor in Fig. 4.3.2.3A, the correlation is high with the Marsta measurements, even though the average of the OML estimates is about 10% below that of Marsta. For the FMI estimates in Fig 4.3.2.3B it is again seen that the values divide into two groups, one for near-zero values, and another one for positive values. The probable explanation for this phenomenon is again the missing sunshine data, as explained in section 4.3.2.4 for the sensible heat flux. For the FMI scheme, the upper cut-off value is about 200 W/m^2. Thus, the two preprocessors correlate well for the near-zero fluxes, which is in good agreement with the high-latitude winter results in Fig. 4.3.1.5, but a poor correlation is found for the positive fluxes where shortwave radiation plays an important role (Fig. 4.3.2.3E).

4.3.2.6 Monin-Obukhov length

The Monin-Obukhov length L is obtained by combining the parameters of friction velocity and surface sensible heat flux. The Monin-Obukhov length is most easily evaluated by observing the frequency with which various values of the inverse 1/L occur. The results are seen in Fig. 4.3.2.4, and compare well with the theoretical comparison shown in Fig. 4.2.4. Furthermore, the frequency distribution for the two measurement sites Marsta and Tisby in Figs. 4.3.2.4A-B is quite similar, with Tisby containing a slightly higher frequency for the near-neutral cases on the stable side.

Overall, the calculations of OML and FMI compare well with the measurements. However, two points should be mentioned. Firstly, the OML preprocessor in Fig. 4.3.2.4C contains a sharp spike at the value of $1/L = 0.5\ m^{-1}$. The reason for this occurence is that during near-neutral situations on the stable side, with values of $L < 100 \cdot z_0$ - where z_0 is the roughness length - OML automatically increases the value to $L = 100 \cdot z_0$. In this way the stability is limited, so extremly stable situations (wich can cause numerical problems in the preprocessor) are not possible. In our case, $z_0 = 0.02$ m, leading to a value of $0.5\ m^{-1}$ for 1/L, corresponding to the spike seen in the figure. Secondly, the FMI scheme gives a slower decline of the frequencies on the stable side (Fig. 4.3.2.4D) as compared both to the measurements and to the OML scheme (Fig.4.3.2.4C). This implies that the FMI scheme will produce more stable situations than OML, which agrees well with the findings in Fig. 4.2.4.

4.3.2.7 Summary of comparisons

The comparisons show that the measurements at the two different sites correlate well for all parameters. As for the calculated values, the preprocessor estimates of the friction velocity have a good agreement with measurements, and the two preprocessors have an extremely high correlation with each other. For the surface sensible heat fluxes, the calculated values tend to be lower than the measured ones. The OML preprocessor, in general, is in good agreement with measurements. However, for both near-zero as well as for higher heat flux values, OML tends to give lower values than measured. The FMI scheme produces good results for the near-zero fluxes during nighttime cases or overcast skies, while the estimates are poor for positive fluxes during daytime clear-sky cases with a higher incoming solar radiation. The cause for the low accuracy FMI results is believed to be the missing sunshine information needed for the net radiation calculation. Overall, the OML and FMI models correlate well for near-zero fluxes, even though the OML values mostly are lower here than the FMI estimates. However, the schemes deviate substantially for positive fluxes during episodes with incoming solar radiation. For net radiation, results are similar to those for the sensible heat flux. Finally, for the inverse Monin-Obukhov length, it is found that the frequency distributions of both measurements and calculations show similar structures. The OML estimates, however, indicate a frequent occurence of the value 0,5 m^{-1}, which is found to be caused by the algorithm which prevents extremely stable situations from occuring. It is also seen that the FMI scheme gives a slower cut-off behavior for near-neutral situations on the stable side than the measurements and the OML preprocessor.

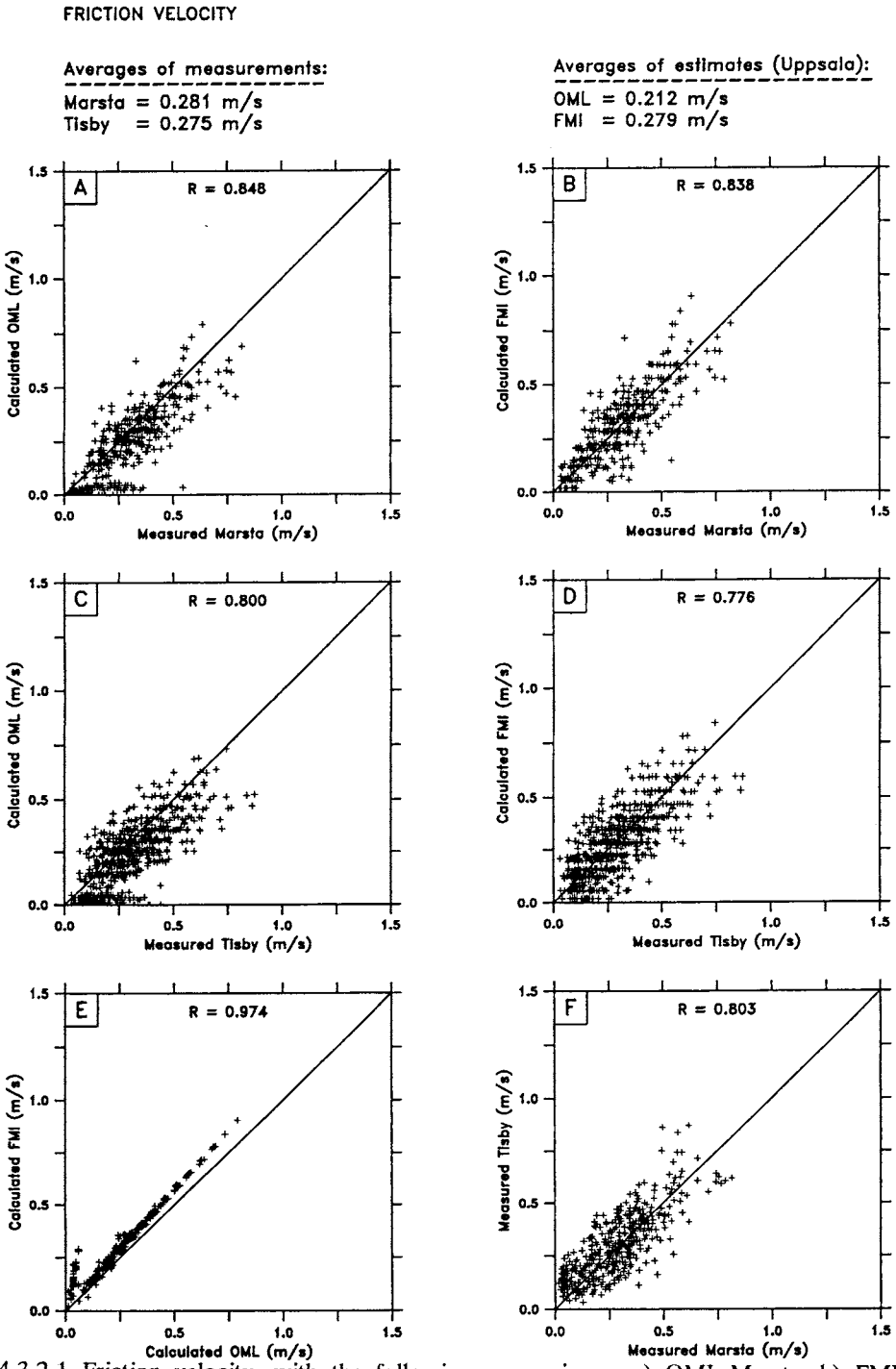

Fig. 4.3.2.1 Friction velocity, with the following comparisons: a) OML-Marsta, b) FMI-Marsta, c) OML-Tisby, d) FMI-Tisby, e) OML-FMI, and f) Marsta-Tisby. The correlation coefficients are given by R. Average values found at top of figure.

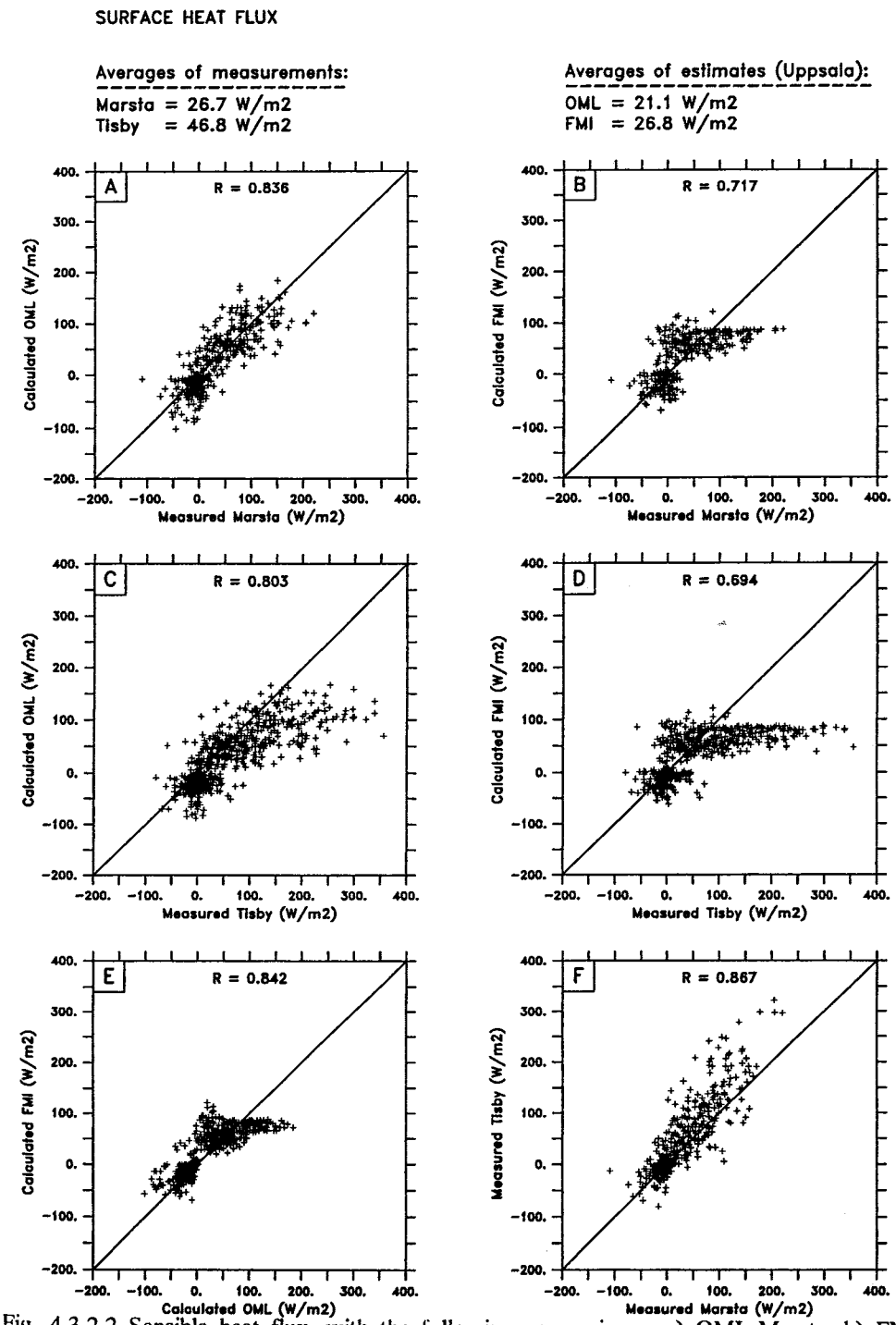

Fig. 4.3.2.2 Sensible heat flux, with the following comparisons: a) OML-Marsta, b) FMI-Marsta, c) OML-Tisby, d) FMI-Tisby, e) OML-FMI, and f) Marsta-Tisby. The correlation coefficients are given by R. Average values found at top of figure.

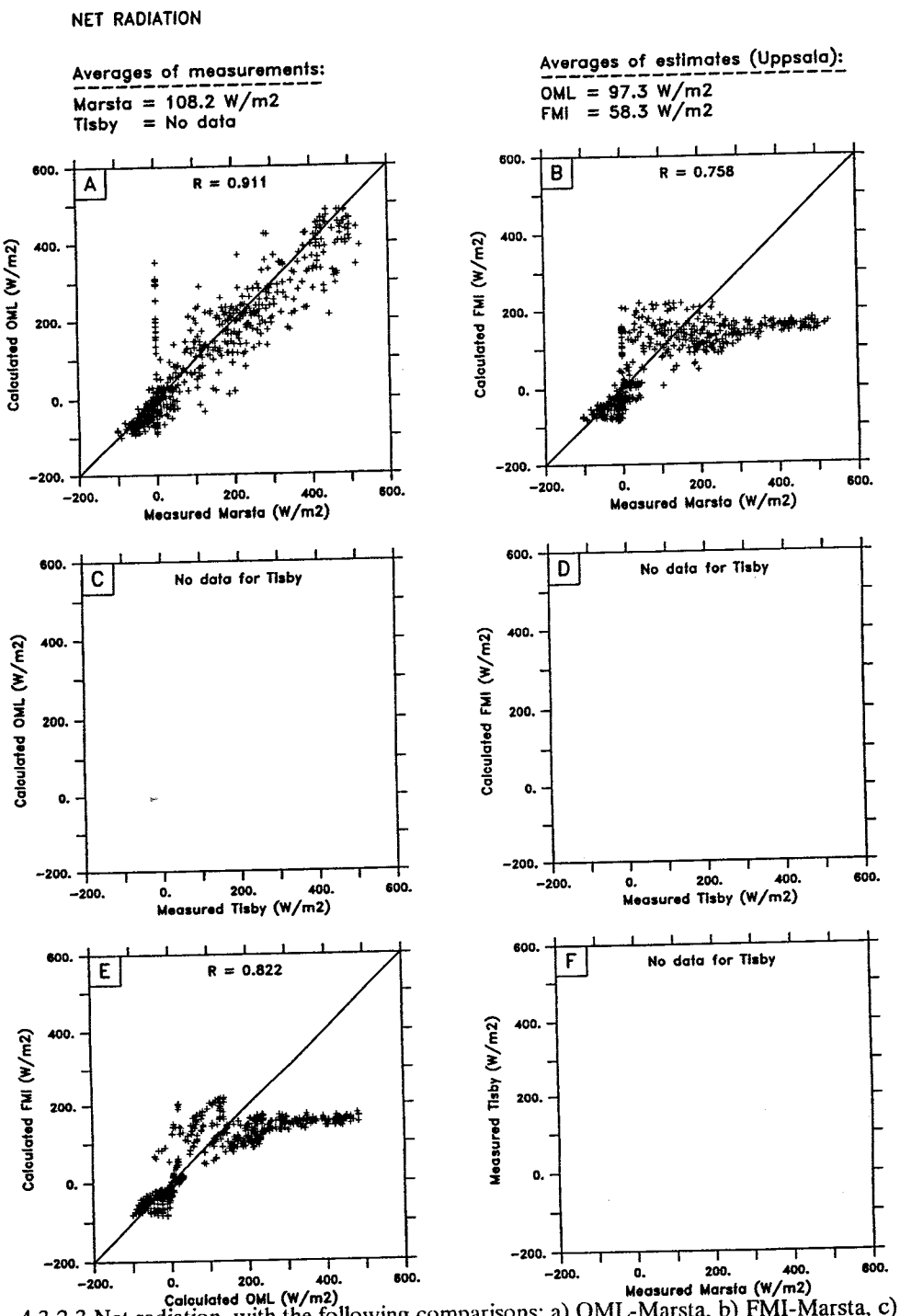

Fig. 4.3.2.3 Net radiation, with the following comparisons: a) OML-Marsta, b) FMI-Marsta, c) OML-Tisby, d) FMI-Tisby, e) OML-FMI, and f) Marsta-Tisby. The correlation coefficients are given by R. Average values found at top figure.

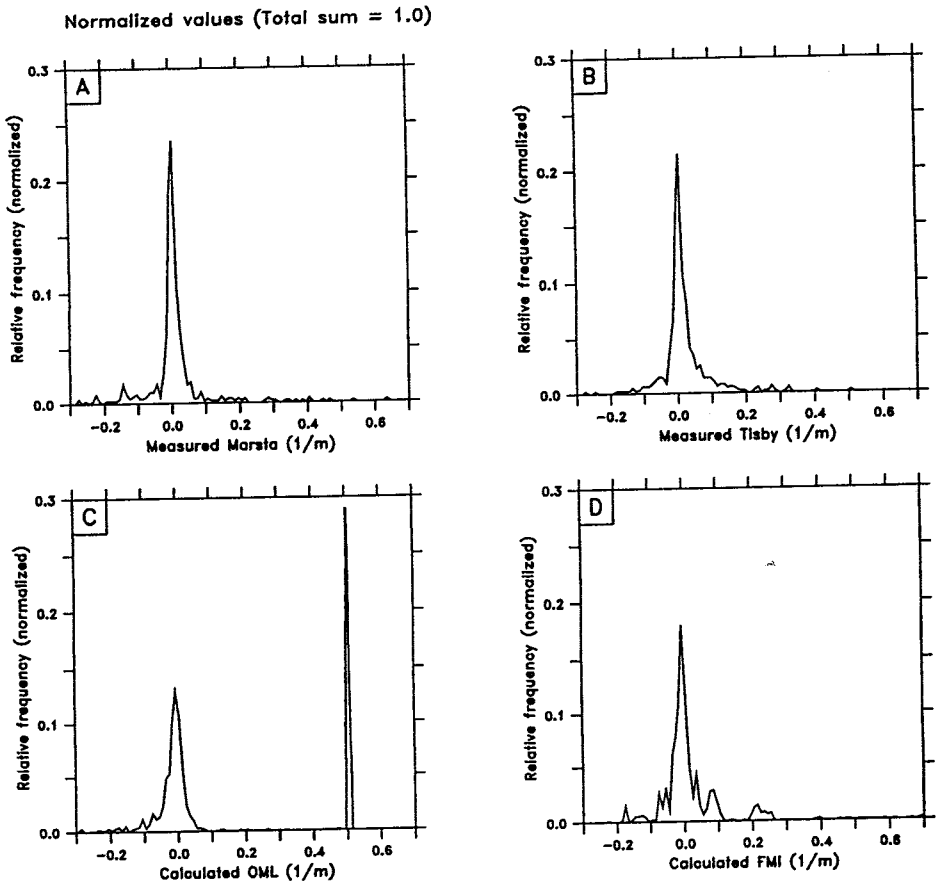

Fig. 4.3.2.4 Inverse Monin-Obukhov length frequencies for the following: a) Marsta, b) Tisby, c) OML, and d) FMI.

4.3.3 Intercomparison of profile method with data

Comparisons of the profile method with data have been studied by numerous authors (Zilitinkevich and Chalikov, 1968; Webb, 1970; Dyer and Hicks, 1970; Businger et al, 1971; Garrat, 1977; Wieringa, 1980, Dyer and Bradley, 1982; Webb, 1982; Foken and Skeib, 1983; Hogstrom, 1985; Hogstrom, 1988; Zhang et al, 1988,) and seem to give good results if the method is used in good conditions.

- accurate measurements near the ground in the SL by taking care of flow disturbance by instrumentation
- good horizontal homogeneity of the site

But, in fact, these optimal conditions are not always respected and necessary data are not always available.

In that way, a comparison study between the resistance and profile methods has been achieved by Rioux and Musson-Genon (1995) by using data collected during a boundary layer experiment focused on pollution events in the Paris area. During this experiment, one site in the surrounding of Paris was instrumented with a LIDAR, a SODAR, a sonic anemometer, and a classical meteorological surface station. Nevertheless, only a screen level temperature was directly measured by a thermometer.

So, for the profile method, a temperature at z_{ot} (thermal roughness height) has been reconstructed with the measurement of infra-red radiation emitted by the earth's surface.

Due in part of the strong dependence of IR radiation on temperature and to the difficulty to obtain a good estimation of z_{ot} it seems difficult to conclude, since the profile method is not applied in good conditions.

4.4 INTERCOMPARISON OF CALCULATED GROUND HEAT FLUX WITH DATA

The following results are restricted to the sensor configuration recommended by the supplier of the ground heat flux device. Different setting (e.g. position of the sensor in the soil, chap.2.5.1) could affect the conclusions (Muehlemann, 1996).

4.4.1 Diurnal cases

A series of selected diurnal variations are used to compare the ground heat flux at the surface, calculated with different parameterization schemes with measurements. Three meteorological clear day situations with rather weak wind have been chosen: two warm episodes in September and October and one cold period in November. The results presented in figure 4.4.1 can be summarized as follows.

Using the proportionality models, the measured ground heat flux is underestimated by about a third of its value. Stull (1989) noted that the proportionality constants are linked to specific conditions and should not be looked upon as universal constants. The factors undergo, in our experiments, strong variations within the selected periods. The ground heat flux can be estimated with a better accuracy when the appropriate factor is available. The site dependence of these models is probably not negligible.

The Arya model requires a sinusoidal distribution of radiation. But heat flux maxima at night of the same order of magnitude as those in daytime don't occur regularly. The model would be probably better adapted for the parameterization of the much larger annual temperature and heat flux cycles.

The Stull's two-layer parameterization of the ground heat flux (force-restore model) gives generally correct estimates of the amplitude of the ground heat flux. A precise knowledge of the soil temperature at a depth where short term (few days) oscillations become negligible or within a tolerable limit is required. The seasonal dependence of this temperature must be introduced. In Figure 4.4.2 this temperature is allowed to be determined as a function of the time of the year. Knowing the actual diurnal amplitude of the surface temperature, one can determine the diurnal damping depth (left panel). The right panel gives then the monthly average measured temperature at this depth. In cold periods, when the top soil freezes, the diurnal amplitude of the top soil temperature tends to zero and $T_m \sim T_G$.

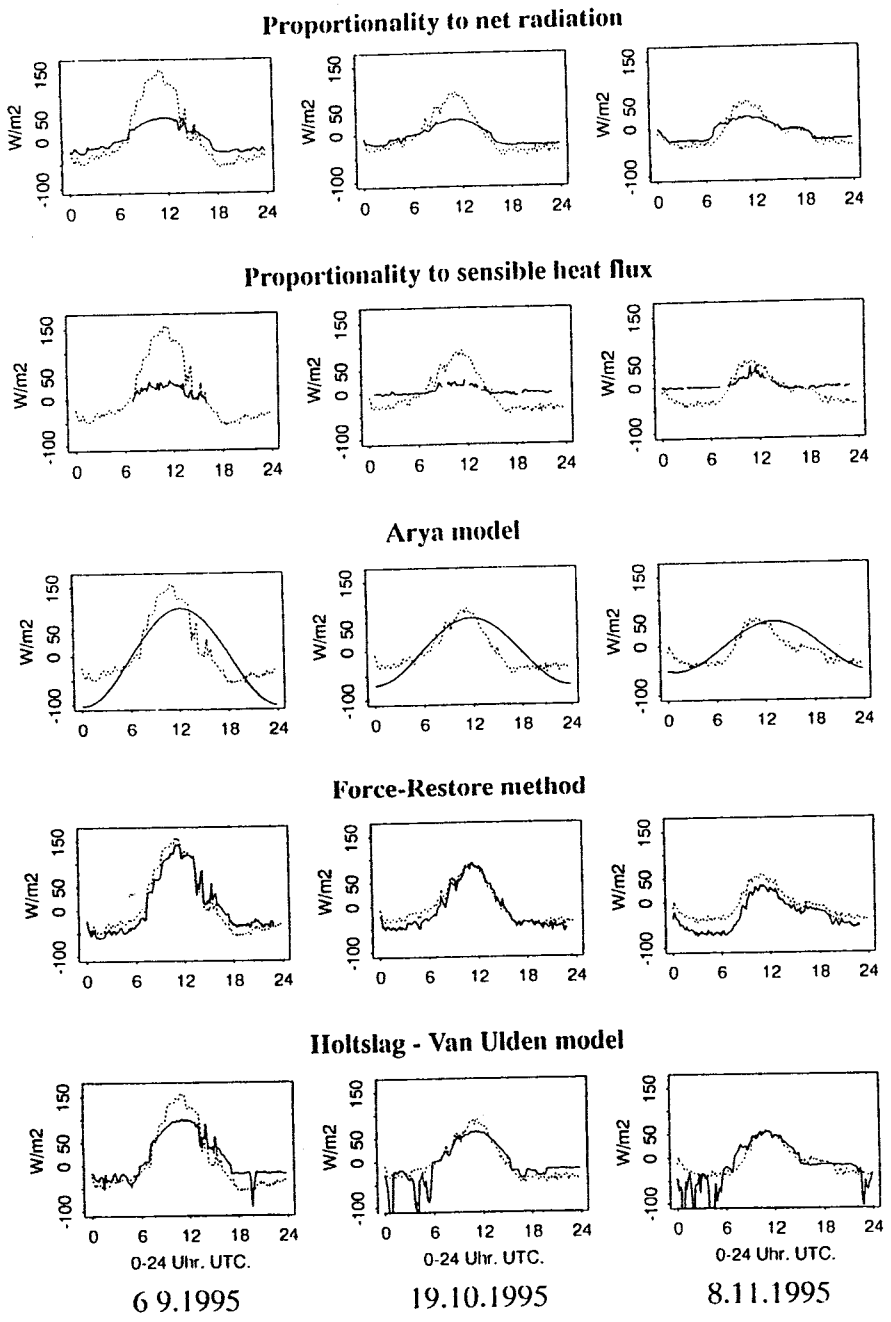

Fig. 4.4.1 : Diurnal variations of the measured (shaded lines) and the calculated (solid lines) ground heat flux at the surface. Comparison for three days and 5 methods.

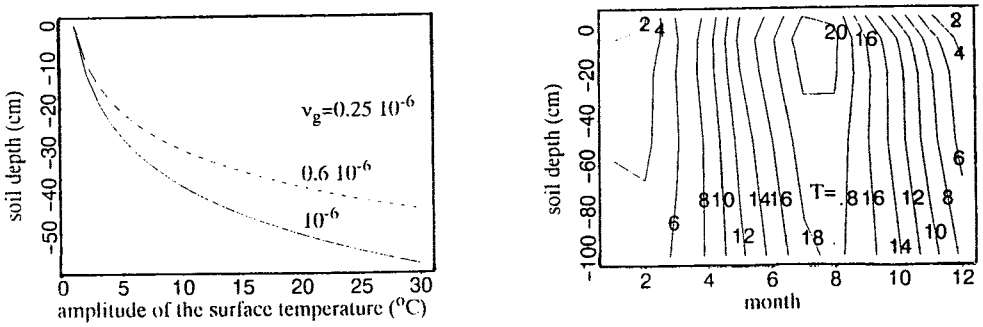

Fig. 4.4.2 : **Left**: depth in the soil at which the diurnal amplitude of the temperature is equal to one degree C for a given amplitude at the surface and for 3 values of the soil thermal diffusivity. **Right**: annual variation of temperature in the soil, ANETZ-station Payerne (average over 6 years)

The structure of the Holtslag - van Ulden model implies a separate discussion of the comparison results for day- and night-time. The daytime ground heat fluxes for the periods were generally estimated with a precision of 10% or better. But underestimations by about 30% occur also. Night-time ground heat fluxes are estimated from Monin-Obukhov similarity theory. The results are therefore dependent upon the inherent correctness of this procedure. This does not seem to be the case at "low" wind speeds. The precise value of "low" seems to be around 2 m/s, but must be considered in relation with the other parameters.

4.4.2 Statistical results

As reported in chapter 2.5.2, proportionality factors are proposed for the determination of ground heat flux at the surface using time series of net radiation. Figure 4.4.3 (left panel) gives the statistical correspondence between one year time series of ground heat flux and net radiation adjusted with the proportionality factors of 0.1 (day) and 0.5 (night). The coefficients given in Figure 4.4.3 (right panel) are estimated from a linear best fit applied on these two series. The nocturnal data require a proportionality factor which does not differ much from the value found in the literature. The daytime value of 0.1 seems to be low compared to the value estimated from the linear fit. It is certainly so because the relation between net radiation and the ground heat flux at the surface is site dependent, especially in daytime.

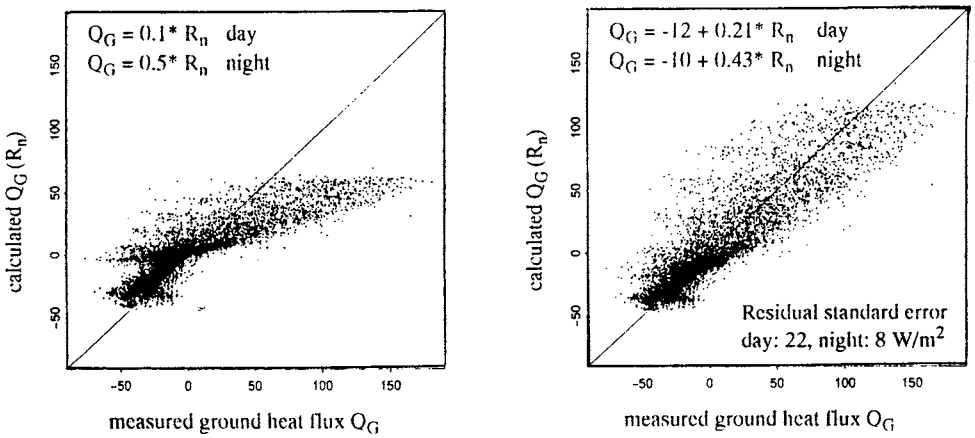

Fig. 4.4.3 : **Left**: ground heat flux at the surface determined from measured net radiation with the commonly proposed proportionality factors of 0.1 for the day and 0.5 for the night versus measured ground heat flux at the surface. **Right**: linear best fit between measured net radiation and measured ground heat flux at the surface . The day-night limit is given by the value of the total incoming radiation > 5 W/m^2. Measurements taken at Payerne from August 1995 to July 1996.

The force-restore method presented in chapter 2.5.2 is a simple way to estimate the diurnal evolution of the ground heat flux at the surface with a sufficient accuracy over the year. For the calculations, the following approximations are introduced :

- the annual average and amplitude of the surface temperature obtained by the temperature measured at 5 cm over the surface.

- the temperature of the shallow slab of soil T_G measured at 5 cm below the surface.

The way to determine the temperature of the thick bottom slab (T_m in the relation 2.5.4) or/and to choose the depth, at which this temperature has to be provided for an optimal estimation of Q_G, does not seem very clear for the two-layer model. Using a constant temperature for T_m at a fixed depth where oscillations are negligible (e.g. 0.5 m or more) overweightes the effect of the deep soil layer when the top soil freezes. The seasonal dependence and also the dependence to the large temperature change induced by weather fluctuations, should be introduced to improve considerably the results. The analytic solution of the thermal wave propagation in a homogeneous soil with the surface temperature simulated as a sinusoidal function of time (annual period) does not replicate these fluctuations.

The left panel of Figure 4.4.4 compares the result of the model using only the seasonal dependence of T_m. The correspondence is as expected relatively poor. A noticeable improvement is obtained by reducing the restore-term by a factor of 2. The correlation increases then from 0.6 to 0.8. The determination of T_G in the restore-term as an average between measurements made at 5 cm above and below the surface also introduces an improvement. Additional linear regression, performed separately for day and night, gives a correlation over 0.9 with a residual error of about 15 W/m^2, respectively 5 W/m^2 but makes then the model site dependent. The right panel of Figure 4.4.4 gives the result of the comparison when T_m is given by the measured soil temperature at 10 cm. This shows that by the determination of hourly ground heat flux T_m and T_G must be never disconnected.

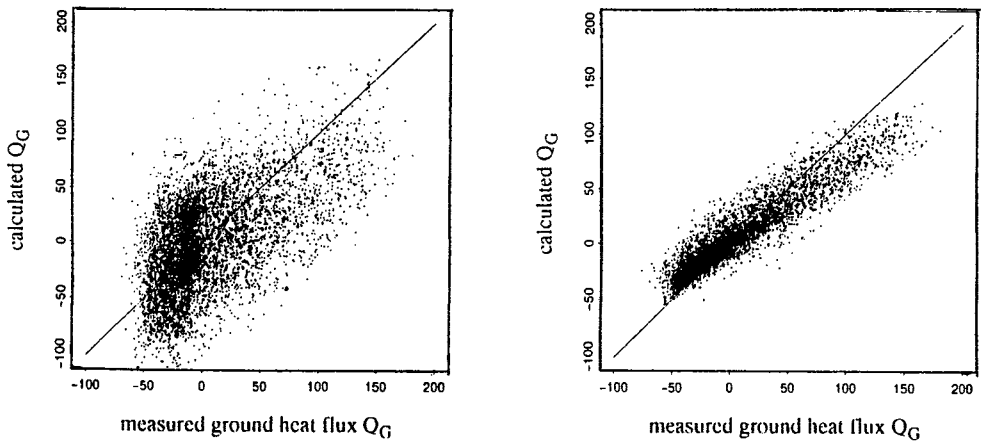

Fig. 4.4.4 : **Left**: ground heat flux at the surface determined with the force-restore method using a sinusoidal function for T_m versus measured ground heat flux at the surface. **Right**: same as left, but using the measured soil temperature at 10 cm for T_m . Measurements taken at Payerne from August 1995 to July 1996.

In summary in order to use the force-restore method to estimate the hourly ground heat flux at the surface with sufficient accuracy, it is necessary to have a measurement of the soil temperature representative of the top layer. More physics should be included into the determination of the ground heat flux Q_G; however the use of the force-restore method for the determination of Q_G can be recommended.

5. LIMITATIONS

The availability of adequate meteorological input data for dispersion modelling often is a problem. Even if data exist, it is sometimes not easy to decide, whether they fit the needs of a given situation. So, before using a method or model, it is always necessary to check the validity of the available input data. Some of the most important problems with input data, although not answered in detail, shall be mentioned in the following subchapters.

REPRESENTATIVENESS

Representativeness with respect to time and to horizontal space:

Time and length scale of the application af a dispersion model determine the resolution of the input data needed.

Each meteorological measurement/observation has as a different representativeness depending on various circumstances, as there are the

- parameter itself (e.g. a cloud cover observation used for parameterizing components of the radiation budget has a rather wide representativeness in space and time compared to an instantaneous wind measurement, especially in complex terrain and an unstable planetary boundary layer)
- siting of the measuring instrument (obviously, measurements may be influenced by buildings or vegetation)
- frequency of measurements and construction of mean values as output of an observation (in the case of high frequent measurements e.g. with sonic anemometer up to 20 Hz, it is important to choose appropriate time intervals and methods for the extraction of mean values and variances)
- application purpose (e.g. single case or statistical application; generally single case studies need more detailed input data than statistical applications)
- weather situation (especially for single case studies; e.g. the variability of meteorological parameters is much greater in a frontal zone than in an anticyclonic influenced region)

The various problems connected with the assessment of meteorological input data are addressed by many authors, e.g. Hanna and Chang (1992), Wieringa (1993), King (1989), Nappo (1983), Weill (1981), Wood (1977), Pruchnicki (1977).

The methods presented here give local determinations of turbulent fluxes and Monin Obukhov length to be used for defining turbulence parameters in Gaussian dispersion models. Therefore these methods should be used in the vicinity of the measurements under the condition of local horizontal homogeneity. This is valid for flat landscape, but certainly not in case of significant orography. Orography may lay enormous restrictions to the representativeness of meteorological measurements. Working group 4 is covering these problems.
Urban areas need special attention within the problem of complex topography. Concerning the task of determining the surface enrgy balance in urban areas, no operational tools are available at present. This is also true for snow covered surfaces.

ROUGHNESS HEIGHT

The right determination of the roughness height z_0 is important for the accuracy of the different methods mentioned in the report.
For terrain where roughness is very variable in space we have to determine an effective roughness that gives the averaged fluxes for the area of interest (Mason, 1988).

In the case of z_0 determination from wind measurements, the concept of blending height (i.e. the height at which flow changes from equilibrium with the local surface to independence of horizontal position (Garratt, 1994)) has to be used (Mahrt, 1996).

In the case where the profile method is used with surface temperature deduced from radiation measurements, the concept of thermal roughness height z_{0t} is needed, even thus atmospheric models often inappropiately assume that z_{0t} is identical to z_0.

SURFACE LAYER HEIGHT

The height of the surface layer, defined as the altitude where the fluxes have decreased less than twenty percent from their surface value, is depending on stability and an estimation can be useful to be sure that the data used to determine the fluxes are really within the surface layer.

For the siting of measuring instruments it is important to remain within the surface layer, especially under stable conditions, when the surface layer might be very shallow.

Other limitations

MO - theory is only valid in the surface layer. The MO - theory may not be valid under very stable conditions with low wind speed.
There is a lot of uncertainty in the determination of the surface energy balance in urban areas.
Only few data on surface energy balance are available for snow covered surfaces.

6. SUMMARY OF RESULTS

Working group 1 has investigated methods for parameterizing the components of the surface energy balance, such as the atmospheric heat, momentum and moisture fluxes and the ground heat flux under horizontally homogeneous conditions.

In one study (section 4.2.1-2), the FMI- and the SMHI- scheme (based on the HU- and BP-schemes, respectively) were intercompared. This study aimed to investigate the properties of the two schemes relative to each other, and did not involve direct comparisons with observations:

Net radiation, estimated with the two schemes, compares well under cloudy sky conditions. When the sky is clear or overcast, the SMHI (BP) scheme predicts up to approximately 20 % larger values of net radiation than the FMI (HU-based) scheme during the day and up to 30 % smaller values of net radiation during the night. Differences in net radiation are the largest under clear sky conditions: during daytime, the difference increases with increasing solar elevation; during night-time and with temperatures below 5°C, the difference increases with decreasing temperatures (minimum temperatures around -20°C). However, comparing quantile - quantile distributions of calculated net radiation from the FMI and OML (BP) scheme for one year of data from Southern Finland, both methods give very similar results for the net radiation.

The quantile - quantile distributions of the calculated sensible heat fluxes differ significantly between the FMI and the OML model. Although the basic input data are identical and the net radiation distributions are nearly the same, the OML model gives consistently lower sensible heat flux values for stable and unstable conditions. The results suggest, that the two parametrization schemes divide differently the available energy between the latent and sensible heat fluxes. It is difficult to determine the wetness of the soil by only using meteorological data. Only the number of cases with positive and with negative sensible heat flux values estimated by the two models is roughly the same. The BP scheme impedes the growth of $1/L_*$ under stable conditions, while the FMI model can generate 'super stable' conditions.

Galinski and Thomson (1995) compared the original HU and BP schemes and a third one (Smith, 1990) with almost three years of measurements from Cardington in UK. During the daytime, all three schemes are based on the surface energy balance, during the night-time only the scheme of Berkowicz and Prahm. The other two schemes estimate the nocturnal heat flux directly. In the intercomparison study of Galinski and Thomson the three daytime net radiation schemes gave quite similar results. Their general conclusion was that for daytime conditions all three schemes give useful correlations for sensible heat flux. All three schemes showed a

tendency to underpredict high sensible heat flux values, in particular for the HU method. Galinski and Thomson attributed this tendency to the fact, that during dry summer months soil moisture and water loss by transpiration is not treated properly (or at all). During daytime the Berkowicz and Prahm heat flux scheme performed best. The use of measured net radiation data in place of derived data did not make a large difference in the results. During night-time the scatter was larger in all three schemes. The Holtslag and van Ulden scheme performed best during the night-time.

An intercomparison of the FMI (HU) and SMHI (BP) scheme with three months of data from Umeå airport in Sweden for high latitude, stable, low wind, winter conditions was carried out (section 4.3.1). The calculated friction velocities show a high correlation between the two schemes. The FMI scheme results in higher values of u_*, which is mainly due to the differences in the roughness length. The FMI scheme assumes a value of 5 cm for snow covered ground, the SMHI scheme 1 cm.

Neither the SMHI (BP) nor the FMI (HU-based) methods seem adequate for prediction of sensible heat flux under the winterly conditions of the experiment. For both schemes the calculated heat fluxes are lower than measured, and there is a poor correlation with measurements. There is a large disagreement between the two schemes. The poor correlation indicates that some important parameter or physics is missing in the schemes for snow covered ground at low temperatures. One reason may be that both schemes fail to reproduce proper values of net radiation which is a crucial parameter for the determination of heat flux. The parametrization of net radiation gives too low values due to the estimation of too high outgoing long wave radiation at very low temperatures. Furthermore, the surface albedo value used in the schemes should be reduced from the values valid for homogeneous snow to make it representative for a larger area. Until better parametrizations of net radiation in this type of winterly conditions become available, it must be recommended to use measured values of net radiation wherever possible.

The high-latitude spring and summer data from central Sweden (section 4.3.2) obtained during four months from the NOPEX campaign lead to conclusions consistent with the earlier results. For daytime cases with low amounts of clouds the underprediction of the HU scheme (in the FMI implementation) is more pronounced than it was in the study by Galinski and Thomson. Here, the FMI heat flux estimates show an upper cut-off value of about 100 W/m^2. This can - at least in part - be ascribed to an underprediction of net radiation. The FMI method needs hourly sunshine duration data for the estimation of net radiation. If these data are not available (as in this study), the FMI scheme calculates the shortwave component as a function of cloud cover by using a regression equation deduced from 10-year measurements in Finland. The

problem with net radiation in the FMI method can possibly be alleviated, if the method is used with the data on hourly sunshine duration, as it was originally designed for.

During night-time conditions, according to Galinski and Thomson, both the HU and the BP scheme have a tendency to underpredict sensible heat flux. This tendency is particularly pronounced for the BP scheme. Such behaviour is consistent with the findings from high-latitude spring and summer data considered here.

Intercomparisons between the resistance and the profile method with data from the Paris area did not provide conclusive results due to experimental shortcomings (section 4.3.3).

Ground heat fluxes, calculated with five schemes, are intercompared with Swiss data from three clear, weak wind days in autumn (section 4.4). The proportionality schemes underestimate the measured ground heat flux by about a third of its value. For clear weather and scattered cloud conditions, the Arya (1988)-model, which assumes a sinusoidal distribution of net radiation, does not reproduce the observed asymmetry of the daily cycle of the ground heat flux. The Stull (1989) force-restore method generally gives correct estimates of the amplitude of the ground heat flux. With the Holtslag - van Ulden model (1983, 1985) the daytime ground heat fluxes are mostly within 10 % of the observed values. For the night-time, the scheme has problems to simulate measured ground heat fluxes under low wind conditions. Intercomparisons with one year of data show that in order to use the force-restore method, it is necessary to have the measured soil temperature with sufficient accuracy. More physics should be included into the determination of the ground heat flux; however, the use of the force-restore method for the determination of the ground heat flux can be recommended.

7. RECOMMENDATIONS

The use of current operational methods is in general acceptable; but the methods do have weaknesses as pointed out in this report, and would benefit from improvements. This is especially the case for winter conditions with snow covered ground.

One should remember that MO theory has been developed for homogeneous terrain. However, a certain inhomogeneity is acceptable, depending on the length scale of the phenomenon with respect to the wall of the flow. Care has also to be taken, when the condition of stationarity is not fullfilled, such as with cumulonimbus clouds, rain, fronts, etc.

The parametrization of the net radiation R_n needs to be improved for snow covered ground and low solar elevations.

Local measurements, either turbulence properties or profiles, should be used whenever possible. In the case there is no local data available, synoptic data can be used, if they are representative for the area of application.

The use of the profile method requires accurate measurements.

There is a need for more data sets to test different parametrization schemes.

More research studies on the use of NWP - models should be carried out: e.g. intercomparison studies between modelled and measured fluxes.

Model output statistics methods should be used to improve BL parameters estimated by NWP models.

Fine mesh resolution models are a promising way to obtain more accurate calculation of BL parameters.

Satellite derived data should be included in the determination of the surface energy balance, if the applicability of the selected parameter has been validated with ground based measurements.

ACKNOWLEDGEMENTS

The authors of this report acknowledge the support given by COST through the Commission of the European Union and the Swiss Government (Philippe Tercier). Warm thanks for making the study with the NOPEX data possible are due to a number of organizers and researchers, especially Jean Labrousse (EC-DG XII), Sven Halldin, Lars-Christer Lundin, Hans Bergström and Magnus Eriksson (Uppsala University) and Sven-Erik Gryning (Risø National Laboratory), who kindly, swiftly and without much bureaucracy provided the measurement data for central Sweden. Further thanks should be extended to Hans Backström (Swedish Meteorological and Hydrological Institute) for putting the synoptic observations at our disposal, and to Helge Olesen (Risø National Laboratory) for providing the meteorological preprocessor computer code. Special thanks also go to Sylvain Joffre and Helge Olesen for their careful reviewing of the report. Last but not least, many thanks to Brigitta Pospisil at the Central Institute for Meteorology and Geodynamics for minutely editing and performing the layout of the manuscript.

ANNEX A

1. INTERNATIONAL COMPARISON OF NWP MODELS

A comparsion between some global NWP models and against climatological evaluations concerning the components of the surface energy budget has been presented by White (1995). Fig. A.1 shows globally and annually averaged values of

- surface evaporation or latent heat flux
- surface sensible heat flux
- net solar radiation at the surface
- net long-wave radiation at the surface
- surface net heat flux

2. SHORT DESCRIPTION OF THE EUROPE-MODELL (EM) AND ITS OUTPUT

The EM is an operational numerical weather prediction Model of Deutscher Wetterdienst (DWD). It covers Europe and a part of the North Atlantic Ocean. Table A 1 shows the main features of the model, including the physical parameterizations and numerical specifications.

The output of EM comprises the components of the atmospheric energy cycle, including the surface layer. Fig. A 2 illustrates the processes within the model; the numbers are mean values over the EM domain and 31 daily forecasts over periods of 24h, starting from +6h up to +30h forecast time (Schrodin, 1996). Principally, the components of the energy balance at the surface can be extracted at each time step of 5 minutes and for of any grid point (horizontal resolution about 55 km) of the model domain.

3. INPUT DATA FOR THE EUROPE-MODELL (EM)

For operational NWP models, a set of grid point values of meteorological parameters has to be determined from the measured and observed data before starting the prognostic iteration. The

steps within this procedure are the numerical analysis, the data assimilation, and the initialization. For the example of the EM, they are described in Tables A 2 and A 3.

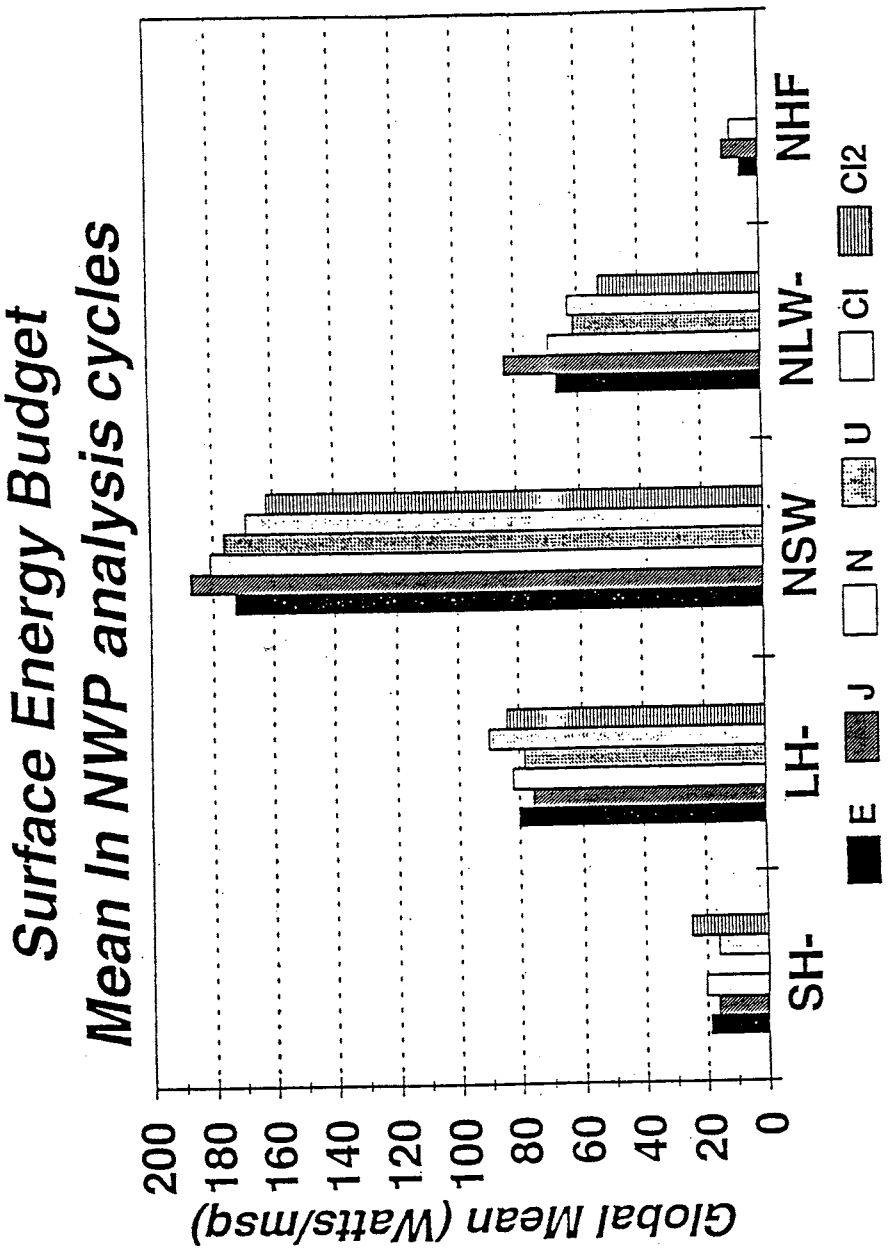

Fig. A 1 Global mean surface energy budget averaged over the 4 seasons. Cl is an annual mean climatology prepared by Ramanathan et.al. (1989), Cl2 are climatological values from Morel (1994). E is ECMWF, J JMA, N NMC(USA), U UKMO, SH sensible heat, LH latent heat, NSW net shortwave radiation, NLW net longwave radiation, NHF net heat flux. Upward fluxes indicated by a hyphen after the abbreviation.

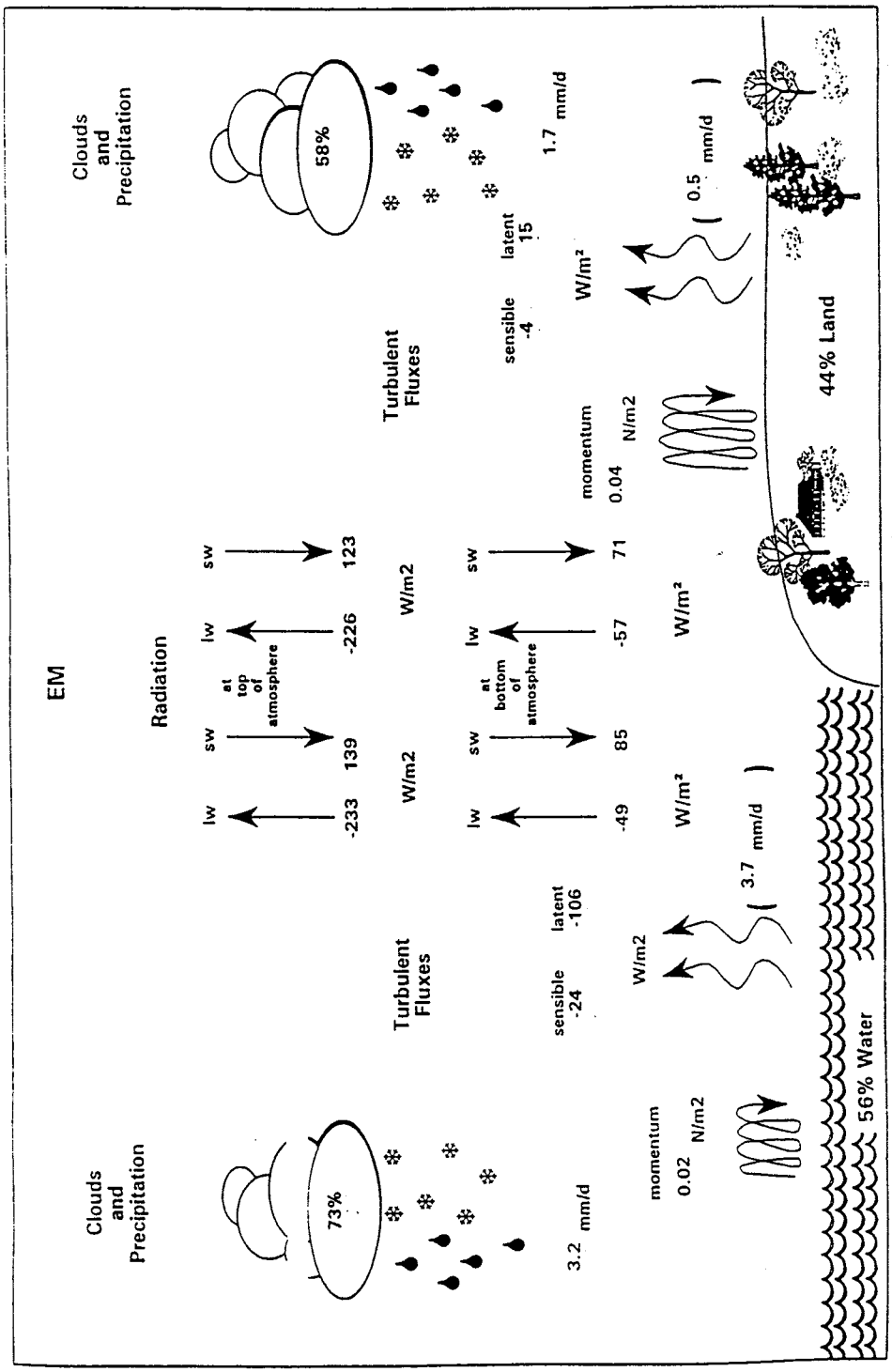

Fig. A 2: Components of the energy cycle for a mean over 31 EM forecasts. Mean over total EM domain and 6 - 30h. 1 - 30 October 1995.

Table A 1: The Europa-Modell (EM) of the DWD.

Europa-Modell (EM)

Hydrostatic meso-α scale regional NWP model for the North Atlantic and Europe.

Prognostic variables
- Surface pressure, total heat, total water content, horizontal wind components.

Diagnostic variables
- Temperature, water vapor and cloud water contents, geopotential, vertical velocity.

Numerics
- Rotated spherical grid, mesh size 0.5° (~ 55 km), Arakawa C-grid.
- Second order horizontal and vertical differencing.
- Hybrid vertical coordinates, 20 layers, 6 layers below 1500 m above ground.
- Semi-implicit time integration, 5-minute time step.
- Lateral boundary formulation due to Davies (1976), boundary values provided by the Global-Modell (GM) at three-hourly intervals.
- Forth-order linear horizontal diffusion, slope-correction for the diffusion of total heat.

Physical parameterizations
- Grid-scale precipitation including parameterized cloud microphysics.
- Mass flux convection scheme after Tiedtke (1989).
- Vertical diffusion after Louis (1979) for the surface layer, an extended level-2 scheme after Mellor and Yamada (1974) higher up.
- δ-two-stream radiation scheme after Ritter and Geleyn (1992) for short- and longwave fluxes, full cloud-radiation feedback.
- Two-layer soil model after Jacobsen and Heise (1982) including snow and interception storage. Climate values changing monthly (but fixed during forecast) in third layer.

Topographic data sets
- Mean orography, land/sea mask and roughness length derived from the 10'·10' NCAR/NAVY data set.
- Prevailing soil type from FAO/UNESCO maps.
- Vegetation cover and root depth from FAO statistics and potential vegetation (2.5°·2.5° resolution).

Operational applications
- forecast: initial dates 00 and 12 UTC; integrations up to 78 hours.
- assimilation cycle: 00, 06, 12 and 18 UTC; integrations up to 6 hours.

Table A 2: Example of data assimilation and analysis of atmospheric fields in NWP models.

Data Assimilation

Method:	6 hourly intermittent data assimilation. Analyses at 00, 06, 12 and 18 UTC 3 separate streams for GM, EM and DM, coupled only via boundary data
Main steps:	Analysis, initialization, forecast (GM-, EM-, DM-Analysis (GA, EA, DA))

Analysis of atmospheric fields

	Mass and wind	Humidity
Method	3D multivariate optimal interpolation (OI) of deviations of observations from 6-h forecasts	3D univariate OI in the troposphere below 250 hPa. Constant specific humidity in the stratosphere
Analysed variables	Geopotential height, wind components, surface pressure	Relative humidity
Constraints	Analysed corrections locally approximately nondivergent and geostrophic	
First guess	6 hour model forecast	
Forecast error correlation	Product of a horizontal and a vertical part.	
	Horizontal model: Series of Besselfunctions Component length scale (middle latidutes): 400 km (GA), 240 km (EA, DA)	$\mu_{ij} = e^{-\frac{1}{2}\frac{r_{ij}}{r_o}}$, $r_o = 300km$
	Vertical model: Empirical positive definite functions	
Observations	SYNOP, SHIP: Pressure. Winds from ships and from tropical landstations	Temperature and dewpoint. Total cloud amount and precipitation.
	TEMP, PILOT: Geopotential heights, winds GA: Only standard levels EA / DA: Additional significant levels	Temperature and dewpoint. Standard levels and significant levels up to 275 hPa
	SATOB: Winds. Not used over extratropical land areas	Upper troposphere humidity (UTH)
	SATEM: Thickness data at 500 km resolution. Not used over land below 100 hPa.	Precipitable water content for 3 layers
	AIREP, ASDAR: Winds	
Observation time window	± 3 hours	
Quality control	Comparison with first guess, comparison with OI analysis	
Realisation	Box method: Simultaneous analysis of a large number of data (up to 500) in large partial volumes of the atmosphere	

Table A 3: Example of data assimilation, analysis of surface parameters, and initialization in NWP models.

Analysis of surface parameters

	Sea surface temperature (SST)	Snow depth
Analysis frequency	Daily at 00 UTC	6 hourly at 00, 06, 12 and 18 UTC
Method	Correction method. Increment calculation at gridpoints with local data selection. Influence radius: 450 km (GA), 350 km (EA), 200 km (DA)	Weighted average at gridpoints with local data selection. Influence radius: 330 km (GA), 250 km (EA), 200 km (DA)
Weights given to observations	a) Dependent on distance b) Dependent on age of observations	Dependent on horizontal and vertical displacement
Observations	SST-data from ships and buoys of the last 7 days	SYNOP snow depth observations. Snowfall data derived from SYNOP precipitation, temperature and weather observations of the last 6 hours
Quality control	Comparison with first guess and with nearby observations	Plausibility checks. Comparison with previous analysis
First guess	Previous analysis	Previous analysis
Adaption in data sparse areas	GA: Blending with SST analysis from NMC Washington EA: Blending with the global analysis DA: Blending with the Europe analysis	Use of snow depth forecast
Ice mask	GA: Ice edge data from NOAA / NAVY Joint Ice Center are used to create the ice mask in the GM-grid EA/DA: Derived from the global ice mask	
Smoothing	2-D smoother is applied to the analysed field	

No analysis of soil temperatures and water contents is performed, but the 6-hour first guess fields are taken

Initialization

GM:	Non-linear normal mode, 5 vertical modes, non-adiabatic
EM/DM:	Implicit non-linear normal mode, 3 vertical modes, adiabatic

ANNEX B

8. LIST OF REFERENCES

Andre, J.C., Bougeault, P., and J.P. Goutorbe, 1990: Regional estimates of heat and evaporation fluxes over non-homogeneous terrain. Examples from the HAPEX-MOBILHY program. Bound.-Layer Meteor., 50, 77-108.

Arya S.P., 1988: Introduction to Micrometeorology. Academic Press, Inc. London.

Barker, E.M and Baxter, T.L., 1975: A note on the computation of atmospheric surface layer fluxes for use in numerical modelling. J. Appl. Meteor., Vol 14, 620-622.

Beljaars, A.C.M. and A.A.M. Holstag, 1991: Flux parametrization over land surfaces for atmospheric models. J. Appl. Meteor. March 1991, 327-341.

Berkowicz, R. and L.P. Prahm, 1982 a: Evaluation of the profile method for estimation of surface fluxes of momentum and heat. Atmos. Env., 16, 2809-2819.

Berkowicz and Prahm, 1982 b: Sensible Heat Flux Estimated from Routine Meteorological Data by the Resistance Method. J. Appl. Metorol. 21, 1845-1864.

Blackadar, A. K., 1979: High-Resolution Models of the Planetary Boundary Layer, Advances in Environmental Science and Engineering,1, 50-85.

Bolle, H.J. et al (35 co-authors), 1993: EFEDA: European field experiment in a desertification threatened area, Annales Geophys., 11, 173-189.

Businger, J.A., Wyngaard, J.C., Izumi, Y. and E.F. Bradley, 1971: Flux-profile relationships in the atmospheric surface layer. J. Atmos. Sci., 28, 181-189.

Carruthers,D.J.,McHugh,C.A.,Robins,A.G.,Thomson,D.J. and M.R Montgomery, 1994: The UK Atmospheric Dispersion Modelling System: Comparisons with data from Kincaid, Lillestrom and Copenhagen. Proceeding of the Workshop:Intercomparison of Advanced Practical Short-Range Atmospheric Dispersion Models (Manno-Switzerland).

Clarke, R.H., Dyer, A.J., Brook, R.R., Reid, D.G. and A.J. troup, 1971: Boundary Layer Data, Tech. Paper n°19, Div. Meteorol. Physics, CSIRO, Australia.

De Bruin, H. and Holtslag, A., 1982: A simple parametrization of the surface fluxes of sensible and latent heat during daytime compared with the Penman-Monteith concept. J. Appl. Meteor. 21, 1610-1621.

Deeheer-Amissah, A., U. Högström and A.S. Smedman-Högström, 1981: Calculation of sensible and latent heat fluxes and surface resistance from profile data. Boundary-Layer Meteor., 20, 35-49.

Driedonks, A.G.M., Van Dop, H. and W. Kohsiek, 1978: Meteorological observations on the 213m mast at Cabauw in the Netherlands. Proc. Fourth Symp. Meteor. Observ. and Instrum., Denver, Amer. Meteor. Soc., Boston, 41-46.

Dyer, A.J. and B.B. Hicks, 1970: Flux-gradient relationships in the constant flux layer, Quart. J. Roy. Met. Soc., 96, 715-721.

Dyer, A.J., 1974: A review of Flux-Profile Relationships. Bound.-Layer Meteor., 7, 363-372.

Dyer A.J. et al, 1982: An international turbulence comparison experiment (ITCE 1976), Bound.-Layer Meteor., 24, 181-209.

Dyer, A.J. and E.F. Bradley, 1982: An alternative analysis of flux-gradient relationships at the 1976 ITCE". Bound.-Layer Meteor., 22, 3-19.

Foken, T.H. and G. Skeib, 1983: Profile measurements in the atmospheric near-surface layer and the use of suitable universal functions for the determination of the turbulent energy exchange. Bound.-Layer Meteor., 25, 55-62.

Galinski and Thomson, 1995: Comparison of Three Schemes for Predicting Surface Sensible Heat Flux. Boundary-Layer Meteorol. 72, 345-370.

Garratt, J.R., 1977: A review of drag coefficients over oceans and continents, Mon. Wea. Rev., 105, 915-929.

Garratt, J.R., 1994: The Atmospheric Boundary Layer, Cambridge Univ. Press, Cambridge, U.K., 316pp.

Garratt, J.R., G.D. Hess, W.L., Physick and P. Bougeault, 1996: The atmospheric boundary layer - Advances in knowledge and application. Bound.-Layer Meteor., 78, 9-37.

Golder D., 1972: Relations among Stability Parameters in the Surface Layer. Boundary-Layer Meteorol. 3, 47-58.

Goutorbe, J.P. et al (15 co-authors), 1994: HAPEX-SAHEL: A large scale study of land atmospheric interactions in the semi-arid tropics, Annales Geophys., 12, 53-64.

Hanna, S., R., and J.C. Chang, 1992: Boundary-layer parameterization for applied dispersion modeling over urban areas. Boundary-Layer Meteorology 58:229-259.

Hanna, S., R., and J.C. Chang, 1992: Representativeness of wind measurements on a mesoscale grid with station separations of 312 m to 10 km. Boundary-layer meteorology, 60, 4, 309-324.

Hansen,G.K., B.F. Jakobsen and S.E. Jensen, 1976. Simuleret planteproduktion. Hydrotechnical Laboratory, Royal Veterinary and Agricultural College, Copenhagen, 155 pp.

Härkönen, J., Walden, J., Kukkonen, J., Pohjola, V. and Kartastenpää, R., 1996: Comparison of model predictions and measurements near a major road in an urban area. Proceedings of the 4th Workshop on Harmonisation within Atmospheric Dispersion Modelling for Regulatory Purposes, 6-9 May 1996, Oostende, Belgium, 8 p.

Högström, U., 1974: A field study of the turbulent fluxes of heat, water vapour and momentum at a "typical" agricultural site. Quart. J. Royal. Meteor. Soc., 100, 624-639.

Högström, U., 1985: Von Karman's constant in atmospheric boundary layer flow: reevaluated, J. Atmos. Sci., 42, 263-270.

Högström U., 1988: Non-dimensional wind and temperature profiles in the atmospheric surface layer: a re-evaluation. Bound.-Layer Meteor., 42, 55-78.

Holtslag A.A.M. and van Ulden A.P. 1982: Simple Estimates of Night-time Surface Fluxes from routine Weather Data. KNMI Scientific Report, W.R. 82-4.

Holtslag A.A.M. and van Ulden A.P. 1983: A Simple Scheme for Daytime Estimates of the Surface Fluxes from routine Weather Data. J. Clim. Appl. Meteorol. 22, 517-529.

Holtslag A.A.M., 1987: Surface fluxes and boundary layer scaling, models and applications. Koninklijk Nederlands Meteorologisch Instituut, Scientific Reports WR-87-2, de Bilt, 176 p.

Izumi, Y., 1971: Kansas 1968 field program data report, Air Force Cambridge Res. Lab., Bedford, Mass., AFCRL-72-0041, Environ. Res. Papers, n°379, 79pp.

Izumi, Y. and S.J. Caughey, 1976: Minesota 1973 atmospheric boundary layer experimental data report, Air Force Cambridge Research Papers n°47.

Johansson P-E, Karlsson E., Thaning L. and Forsberg B., 1994: Atmospheric Stability and its influence on Air Quality in small communities in northern Sweden. FOA report C 40323-4.5.

Johansson, P., 1996: Comparison between different pre-processors during high latitude winter conditions. Proceedings of the 4th Workshop on Harmonisation within Atmospheric Dispersion Modelling for Regulatory Purposes, 6-9 May 1996, Oostende, Belgium, 7 p.

Karppinen, A., Joffre, S. and Vaajama, P., 1996a: Boundary layer parametrization for Finnish regulatory dispersion models. Proceedings of the 4th Workshop on Harmonisation within Atmospheric Dispersion Modelling for Regulatory Purposes, 6-9 May 1996, Oostende, Belgium, 8 p.

Karppinen, A., Nordlund, G., Rantakrans, E., and Valkama, I., 1996b: Dispersion modelling system for urban air pollution UDM-FMI. Finnish Meteorological Institute, Report. Helsinki, 25 p.

Karppinen, A., Kukkonen, J., Nordlund, G., Rantakrans, E., and Valkama, I., 1997: A dispersion modelling system for urban air pollution. Finnish Meteorological Institute, Publications on Air Quality. Helsinki, 50 p. (in print)

Kerschgens, M. J., 1987: Die Energetik der Stadt, Dümmler, Bonn.

King, C. W., 1989: Representativeness of single vertical wind profiles for determining volume flux in valleys. Journal of applied meteorology, 28, 6, 463-466.

Louis, J.F, 1979: A parametric model of vertical eddy fluxes in the atmosphere. Bound.-Layer Meteor., 17, 187-202.

Louis, J.F., Tiedke, M. and J.F. Geleyn 1982: A short history of the PBL parameterization at ECMWF. Workshop on boundary layer parameterization, november 1981, ECMWF, Reading, England, 59-79.

Majewski, D., 1995: The Workstation-Version of the EM/DM, Deutscher Wetterdienst, Offenbach.

Mahrt L., 1996: The bulk aerodynamic formulation over heterogenous surfaces. Bound.-Layer Meteor., 78, 87-119

Mason, P.J., 1988: The formation of areally averaged roughness lengths. Quart. J. Roy. Meteor. Soc., 114, 399-420.

Mayocchi C.L. and K.L. Bristow, 1995: Soil Surface Heat Flux: Some General Questions and Comments on Measurements. Agricult. and Forest Meteorol, 75, 43-50.

Monteith, J. L., Evaporation and surface temperature. Quart. J. Roy. Met. Soc., 107, 1-27.

Morel, P., 1995: Scientific issues underlying the global energy and water cycle. European Conference on the Global Energy and Water Cycle, London, U.K., 18-22 July 1995.

Muehlemann P., 1996: Vergleich von Parametrisierungen des Bodenwaermeflusses sowie des sensiblen und latenten Waermeflusses in Bodennaehe mit Einbezug der Energiebilanz. Diplomarbeit, Geogr. Inst. der Universitaet Bern.

Myrup, L. O., 1969: A Numerical Model of the Urban Heat Island, J. Appl. Meteorol., 8, 908-918.

Nappo, C. J., 1983: Methods of estimating meteorological representativeness. 5. Symposium meteorological observations and instrumentation, April 11-15, 1983, Toronto, Ont., Canada. Boston, Amer.Meteorol.Soc., 246-252.

Nielsen, L.B., Prahm, L.P., Berkowicz, R. and Condradsen, K.,1981: Net Incoming Radiation Estimated from Hourly Global Radiation and/or Cloud observations. J. Climat.,1, 255pp.

Oke, T. R., 1987: Boundary layer climates, Methuen, London and New York.

Olesen, H. R. and Brown, N., 1992, 2. edition: The OML meteorological preprocessor - a software package for the preparation of meteorological data for dispersion models. MST LUFT-A122. National Environmental Research Institute, DK-4000 Roskilde, Denmark.

Omstedt G., 1988: An Operational Air Pollution Model. SMHI Report RMK 57.

Paulson, C.A., 1970: The mathematical representation of wind and temperature profiles in the unstable atmospheric surface layer. J. Appl. Meteor., .9, 857-861.

Ramanathan, V. et.al., 1989: Climate and the Earth's Radiation Budget, Physics Today 42, 22-32.

Pruchnicki, J., 1977: Method of selecting a meteorological station representative for estimating the wind impact on the spread of air pollution. Z.f.Meteorol. 27, 2, 119-125.

Rioux, M. and L. Musson-Genon, 1995: Determination of sensible heat and momentum fluxes from data measurements of the ECLAP campaign, technical note HE-33/96-009 available at EDF/DER/AEE/ENV, 6 quai Watier 78401 Chatou Cedex, France.

Rioux M. and L. Musson-Genon, 1995: Etude de la reconstitution des flux de chaleur et de quantité de mouvement à partir des données de la campagne ECLAP. Note technique EDF-DER n°HE33/95/016 available at EDF/DER/AEE/ENV, 6 quai Watier 78401 Chatou cedex France.

Roos, C., 1995: Verifikation der Inversionshöhenbestimmung mit dem 1 dimensionalen Grenzschichtmodell von A.K. Blackadar anhand von SODAR-Messungen, Diploma Thesis, University of Cologne.

Schlünzen, K. H., 1994: Mesoscale Modelling in Complex Terrain - An Overview on the German Nonhydrostatic Models, Beitr. Phys. Atmosph., 67, 243-253.

Schrodin, R. (Editor), 1995: Dokumentation des EM/DM-Systems, Deutscher Wetterdienst, Offenbach.

Schrodin, R. (Editor), 1996: Quarterly Report of the Operational NWP-Models of the Deutscher Wetterdienst, No. 5.

Schulz, J. et al., 1995: Evaluations of Satellite-Derived Latent Heat Fluxes, Max-Planck-Institut für Meteorologie, Hamburg, Report No 181.

Sellers, P.J., Hall, F.G., Asrar, G., Strebel, D.E. and R.E. Murphy, 1988: The first ISLSCP field experiment, Bull. Amer. Meteorol. Soc., 69, 22-27.

Sellers, P.J. et al (12 co-authors), 1995: The Boreal ecosystem atmosphere study (BOREAS): An overview and early results of the 1994 field years, has appeared to Bull. Amer. Meteorol. Soc.

Smith B., 1990: Atmospheric Structure. Unpublished note presented at Air Pollution Modelling for Environmental Impact Assessment, International Centre for Theoretical Physics, Trieste, June 1990.

Stathers, R. J. et al., 1988: Modelling Surface Energy Fluxes and Temperatures in Dry and Wet Bare Soils, Atmosphere-Ocean, 26, 59-73.

Stull R.B., 1989: An Introduction to Boundary Layer Meteorology. Atmospheric Sciences Library. Kluwer Academic Publishers.

Todhunter, P. E., and Terjung, W. H., 1988, Intercomparison of Three Urban Climate Models, Boundary Layer Meteorology, 42, 181-205.

Van Ulden, A. and Holtslag, A., 1985: Estimation of atmospheric boundary layer parameters for diffusion applications, J. Climate Appl. Meteor.24, 1196-1207.

Walden, J., Härkönen, J., Pohjola, V., Kukkonen, J. and Kartastenpää, R., 1995: Vertical concentration profiles in urban conditions - comparison of measurements and model predictions. In: Anttila, P. et al. (ed.), Proceedings of the 10th World Clean Air Congress, Espoo, Finland, May 28 - June 2, 1995. Vol. 2. The Finnish Air Pollution Prevention Society, Helsinki, p. 268 (4 pages).

Webb, E.K., 1970: Profile relationships: The log-linear range and extension to strong stability, Quart. J. Roy. Met. Soc., 96, 67-90.

Webb, E.K., 1982: Profile relationships in the superadiabatic surface layer, Quart. J. Roy. Met. Soc., 108, 661-688.

Weill, A., 1982: Measurements in the atmospheric boundary layer; Techniques and limitations, Representativeness. Workshop on planetary boundary layer parameterization, 25-27 Nov. 1981, Reading, ECMWF, 35-57.

Weill et al (31 co-authors), 1988: The MESOGERS-84 experiment: A report. Bound.-Layer Meteor., 42, 251-264.

Wieringa, J., 1993: Representative roughness parameters for homogeneous terrain. Boundary-Layer Meteorology, 63, 4, 323-363.

White, G. H., 1995: An Intercomparison of Precipitation and Surface Fluxes from Operational NWP Analysis/Forecast Systems, WMO/TD-No.723, Geneva.

WMO, Joint Planning Office: Global Climate Observing System, 1995: Plan for space-based observations, Version 1.0, WMO/TD-No.684, Geneva.

Wood, N. L. H., 1977: A field study on the representativeness of turbulent fluxes of heat and water vapour at various sites in Southern England. Quart. J. Roy. Met. Soc., 103, 483, 617-624.

Wotawa, G. et. al., 1996: Parameterization of the Planetary Boundary Layer over Europe - A Data Comparison between the Observation Based OML Preprocessor and ECMWF Model Data, Beitr. Phys. Atmosph., 69, 273-284.

Zhang, S.F., Oncley, S.P. and J.A. Businger, 1988: A critical evaluation of the von Karman constant from a new atmospheric surface layer experiment, in Proceedings of the 8th Symposium on turbulence and diffusion, pp 148-150, American Meteor. Soc., Boston, MA.

Zilitinkevich, S.S. and D.V. Chalikov, 1968: Determining the universal wind-velocity and temperature profiles in the atmospheric boundary layer, Izv. Atmospheric and Oceanic Physics, 4, 294-302 (English version pp 165-170).

9. LIST OF SOME DATA SETS

9.1 List of recognized existing data sets concerning surface energy balance according to recent review paper over boundary layer (Garratt et al, 1996)

HAPEX-MOBILHY	Andre et al, 1990
EFEDA	Bolle et al, 1993
HAPEX-SAHEL	Goutorbe et al, 1994
FIFE	Sellers et al, 1988
BOREAS	Sellers et al, 1995

9.2 List of recognized existing data sets concerning flux-gradient relationships

WANGARA	Clarke et al, 1971
KANSAS	Yzumi, 1971
MINESOTA	Yzumi and Caughey, 1976
LOVSTA	Hogstrom, 1988
CABAUW	Driedonks et al, 1988
MESOGERS	Weill et al, 1988

9. 3 List of some data sets concerning the resistance method

HØJBAKKEGAARD	Hansen et al., 1976
MARSTA	Högström,1974 ; Deheer-Amissah et al., 1981
CABAUW	Holtslag et al., 1983
CARDINGTON	Galinski and Thomson, 1995

4.3. INTERCOMPARISON OF METHODS WITH OBSERVED DATA

4.3.1 Intercomparison of SMHI-scheme and FMI scheme for high latitude winter conditions

The study described in this subsection deals with high latitude winter conditions. The two commonly used preprocessing schemes, the HU (Holtslag and van Ulden, 1982; 1983) and the BP (Berkowicz and Prahm, 1982b) schemes are compared to measurements and to each other during a period of typical high latitude winter conditions.

The implementation of the schemes are, respectively, that of the FMI (Karppinen et al., 1996) which is based on the HU scheme, and that of the SMHI (Omstedt, 1988) which fully represents the BP method. The purpose of this comparison is to investigate how well such meteorological preprocessors perform during typical winter conditions. The purpose of this comparison is to investigate how well such meteorological preprocessors, would perform during typical winter conditions in northern Europe. During winter time at high latitudes the surface is often snow covered with high albedo values, and the incoming solar radiation is small or absent during the whole day. This may result in very stable stratification with low temperatures and low wind speeds - conditions which can prevail for extended periods of time. Such situations are neither rare nor extreme for the northern areas. Furthermore, the concentration of most pollutants reach their annual maximum during the winter.

Measurements

The measurements used for the study were made at Umeå Airport (63°48' N, 20°17' E), just outside the city of Umeå, along the eastern coast of Sweden. The period chosen for this study is from January 18 to March 17, 1994. During the whole period the ground was covered with a layer of snow (≈0.6 m thick), the temperature and wind speed was mainly low, which together with weak insolation gave the desired "stable to very stable" conditions.
Direct measurements of the surface fluxes were accomplished by the use of a Solent sonic anemometer and the eddy-correlation technique. The sonic anemometer was mounted on a small mast at the height of 5 m, and the sampling frequency was set to 20 s^{-1}. Additionally net radiation was measured with a net radiometer (Siemen-Ersking) mounted at 2 m height on another mast close to the first one. The masts were situated in a flat area about 150 m from the runway, which was covered by a thin layer of snow. The closest buildings were about 200 m to the NNE of the masts, and only in narrow wind direction sector. Routine meteorological observations, from the synoptic station at the airport, were made available by SMHI. Measurements of hourly sunshine time, used as input data for the FMI preprocessor, was also provided by SMHI.

Method

The compared parameters were the friction velocity (u_*; or momentum flux) and the surface sensible heat flux (H), since most parameterizations are based on the Monin-Obukhov length scale, L_*:

10. LIST OF SOME PREPROCESSING METHODS WITH AVAILABLE PROGRAMS

Beljaars, A.C.M., and Holtslag, A.A.M., 1990. A software Library for the Calculation of Surface Fluxes over Land and Sea. Environmental Software 5, 60-68.

Hanna, S., R., and J.C. Chang, 1991. User's Guide for the HPDM-4.0 Software Package. The Electric Power Research Institute, 3412 Hillview Avenue,Palo Alto, CA 94303.

Olesen, H. R. and Brown, N., 1992, 2. edition: The OML meteorological preprocessor - a software package for the preparation of meteorological data for dispersion models. MST LUFT-A122. National Environmental Research Institite, DK-4000 Roskilde, Denmark.

PBL-MET LIBRARY : A software library for advanced meteorological and air quality data processing. SERVIZI TERRITORIO S.C.R.L., Cinisello Balsamo, MILAN, ITALY

A workstation version of the EM/DM system is available from DWD, also a detailed documentation including all parameterizations (Majewski, 1995; Schrodin, 1995).

C. Roos and F. Steffany, 1994. Energie-Bilanz-Modell EBiMo, Benutzeranleitung, Institut für Meteorologie und Geophysik, Universität Köln.
The model EBiMo, described in 2.1.2, is available from Kerschgens, University of Cologne.